Heliyon 10 (2024) e30204

Contents lists available at ScienceDirect

Heliyon

journal homepage: www.cell.com/heliyon

Research article

miR-153 promotes neural differentiation by activating the cell adhesion/Ca^{2+} signaling pathway and targeting ion channel activity in HT-22 cells by bioinformatic analysis

Li Jiao [a], Zhang Junfang [a], Li Yanna [a], Jin Caixia [b], Zhang Chen [c], Jia Song [a], Xu Jie [a], Yan Xiaoli [a], Gui Xin [d], Xing Libo [d], Wang Feng [e], Lu lixia [b,***,1], Xu Chunli [e,**,1], Xu Lei [b,*,1]

[a] Teaching Laboratory Center, Tongji University School of Medicine, Shanghai, China
[b] Department of Biochemistry and Molecular Biology, Tongji University School of Medicine, Shanghai, China
[c] Department of Laboratory Research Center, Tongji University School of Medicine, Shanghai, China
[d] School of Life Science and Technology, Tongji University, Shanghai, China
[e] Department of Neurology, The Seventh People's Hospital of Integrated Traditional Chinese and Western Medicine Affiliated to Shanghai University of Traditional Chinese Medicine, Shanghai, China

ARTICLE INFO

Keywords:
miR-153
Bioinformatic analysis
Neural differentiation
Neural cell adhesion
Receptor tyrosine kinase
Ion channel

ABSTRACT

MicroRNAs have been studied extensively in neurodegenerative diseases. In a previous study, miR-153 promoted neural differentiation and projection formation in mouse hippocampal HT-22 cells. However, the pathways and molecular mechanism underlying miR-153-induced neural differentiation remain unclear. To explore the molecular mechanism of miR-153 on neural differentiation, we performed RNA sequencing on miR-153-overexpressed HT-22 cells. Based on RNA sequencing, differentially expressed genes (DEGs) and pathways in miR-153-overexpressed cells were identified. The Database for Annotation, Visualization and Integrated Discovery and Gene Set Enrichment Analysis were used to perform functional annotation and enrichment analysis of DEGs. Targetscan predicted the targets of miR-153. The Search Tool for the Retrieval of Interacting Genes and Cytoscape, were used to construct protein-protein interaction networks and identify hub genes. Q-PCR was used to detect mRNA expression of the identified genes. The expression profiles of the identified genes were compared between embryonic days 9.5 (E9.5) and E11.5 in the embryotic mouse brain of the GDS3442 dataset. Cell Counting Kit-8 assay was used to determine cell proliferation and cellular susceptibility to amyloid β-protein (Aβ) toxicity in miR-153-overexpressed cells. The results indicated that miR-153 increased cell adhesion/Ca^{2+} (Cdh5, Nrcam, and P2rx4) and Bdnf/Ntrk2 neurotrophic signaling pathway, and decreased ion channel activity (Kcnc3, Kcna4, Clcn5, and Scn5a). The changes in the expression of the identified genes in miR-153-overexpressed cells were consistent with the expression profile of GDS3442 during neural differentiation. In addition, miR-153 overexpression decreased cellular susceptibility to Aβ toxicity in HT-22 cells. In conclusion, miR-153 overexpression may promote neural differentiation by inducing cell adhesion and the Bdnf/Ntrk2 pathway, and regulating

* Corresponding author.
** Corresponding author.
*** Corresponding author.
E-mail addresses: lulixia@tongji.edu.cn (L. lixia), xuchunli7775@163.com (X. Chunli), xvleii@163.com (X. Lei).
[1] Lu lixia, Xu Chunli and Xu Lei are co-corresponding authors contributed equally to this study.

https://doi.org/10.1016/j.heliyon.2024.e30204
Received 8 October 2023; Received in revised form 21 April 2024; Accepted 22 April 2024
Available online 26 April 2024
2405-8440/© 2024 The Authors. Published by Elsevier Ltd. This is an open access article under the CC BY-NC license (http://creativecommons.org/licenses/by-nc/4.0/).

electrophysiological maturity by targeting ion channels. MiR-153 may play an important role in neural differentiation; the findings provide a useful therapeutic direction for neurodegenerative diseases.

1. Introduction

There is increasing evidence that microRNAs (miRNAs) regulate neural growth and development [1]. MiRNA ablation at an earlier time point, at embryonic days 7.5 (E7.5), by conditional knockout of DICER, causes overt structural defects in the neuroepithelium by disrupting adherence junctions and inducing hyperproliferation of radial glial cells [2]. Some miRNAs, such as miR-132 and miR-212 promote dendrite growth in vitro and in adult-born hippocampal neurons [3,4]. Dysregulation of miRNAs has been implicated in neurodegenerative diseases, including Alzheimer's (AD), Parkinson's, and Huntington's disease by altering gene expression or signaling pathways of neural growth and differentiation [5]. Inducing neural differentiation and remodeling synaptic function protects or restores neural function and may have potential therapeutic value in neurodegenerative diseases.

MiR-153 has been suggested to be a brain-specific miRNA [6]. Mouse miR-153 is located on chromosome 12. Stappert et al. [7] showed the upregulation of miR-153, miR-324-5p/3p and miR-181a/a* during neural differentiation and their contribution to shifting lt-NES cells (long-term self-renewal neuroepithelial-like stem cells from human pluripotent stem cells) from self-renewal to neuronal differentiation. Qiao et al. [8] also indicated that miR-153 promotes neurogenesis by targeting the Notch signaling pathway and increasing the cognitive abilities of aged mice. In another study [9], miR-153 reduced Aβ in human brain cultures and itself dysregulated in AD compared with control. In our previous study, miR-153 promotes neural differentiation and projection formation in HT-22 cells by increasing the expression of Nse, Neu, Snap23 and Snap25 [10]. Mouse hippocampal HT-22 cells were cloned from HT4 cells that had been grown without establishing synaptic connections [11]. Collectively, miR-153 plays an important role in neurogenesis and the pathogenesis of neurodegenerative diseases. However, the pathways and molecular mechanism underlying miR-153 induced neural differentiation remain unclear.

To reveal the possible molecular mechanism underlying miR-153 overexpression in HT-22 cells, we performed RNA sequencing. High-throughput sequencing (HTS) is a modern technology that has developed over the past millennium. Owing to its advantages of being fast, cost effective and generating substantial amounts of data, HTS is widely used in modern life science research, particularly to provide guidance for further studies [12]. RNA sequencing is an HTS technique used to quantify gene expression profiles. Big raw data produced by RNA sequencing need to be further extracted and analyzed using bioinformatics tools. Here, We used internationally recognized and rapidly updated databases and online tools for further data analysis. Our results demonstrate that miR-153 increases cell adhesion/Ca^{2+} signaling and the Bdnf/Ntrk2 neurotrophic signaling pathway and decreases ion channel activity, which may affect neural differentiation and axon remodeling. Some of the upregulated hub genes identified in cell adhesion and the Bdnf/Ntrk2 pathway, and the downregulated genes in ion channel activity indicated consistent alterations during mouse embryonic brain development between E9.5 and E13.5, by analyzing the gene expression of the GDS3442 dataset. In addition, Cell Counting Kit-8 (CCK8) assay demonstrate that miR-153 attenuated cell proliferation and also decreased cell susceptibility to Aβ toxicity compared with those in the control.

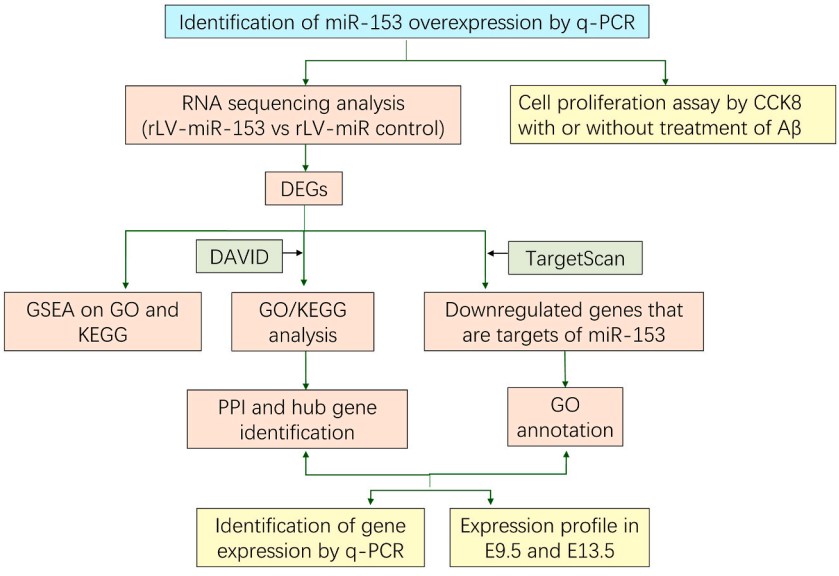

Fig. 1. The flowchart of the study. Effect of miR-153 on HT-22 cells by bioinformatic analysis and experiments. DEGs: differentially expressed genes. E9.5: mouse embryonic days 9.5. E13.5: mouse embryonic days 13.5.

2. Methods

A flowchart of the overall study design is shown in Fig. 1.

2.1. miRNA extraction and quantitative polymerase chain reaction (qPCR)

To identify the expression of miR-153 in stable miR-153-infected cells, miRNA was extracted from, HT-22 cells transfected with miR-153 viral particles (rLV-miR-153) and control cells, HT-22 cells transfected with control viral particles (rLV-miR), and qPCR was performed for analysis. The kits for miRNA isolation (DP501), miRNA First-Strand cDNA Synthesis (KR211) and miRNA qPCR Detection (FP411) were purchased from Tiangen Biotech Co., Ltd (Beijing, China). qPCR reactions were performed in triplicate using the Step One Plus PCR System (Applied Biosystems; Thermo Fisher Scientific, Inc). The data were normalized against the levels of U6 RNA. The sequences of mature mmu-miR-153-5prime (accession no. MIMAT0016992) and mmu-miR-153-3prime (accession no. MIMAT0000163) were used as forward primers for the miRNA qPCR analysis.

2.2. RNA sequencing analysis and data processing of differentially expressed genes (DEGs)

Total RNA was isolated with the TRIzol reagent (Takara) from rLV-miR and rLV-miR-153 cells (three biological replicates for each group). RNA sequencing was performed according to the Illumina standard protocol of Beijing Novel Bioinformatics Co. Ltd. (https://en.novogene.com/). Briefly, a qualified cDNA library was prepared and sequenced using Illumina NovaSeq 6000, and raw reads were generated. The Raw reads were processed using in-house Perl scripts. Clean reads were obtained by removing reads containing adapters, poly-N, and low-quality reads from raw data. After quality control, all downstream analyses were performed using high quality clean data. The Index of the reference genome was built using Hisat2 (version 2.0.5) and clean paired-end reads were aligned to the reference genome using Hisat2 (version 2.0.5). FeatureCounts (version 1.5.0-p3) was used to determine the number of reads mapped to each gene. The FPKM of each gene was then calculated based on the length of the gene and the read count mapped to the gene. Differential expression analysis of the two groups (rLV-miR-153 vs. rLV-miR) was performed using the DESeq2 R package (version 1.20.0). Adjusted p value < 0.05 and $|\log2FoldChange[FC]| \geq 1$ were considered as the cutoff criteria for the selection of DEGs. The complete RNA-seq data in this study was deposited at NCBI (http://www.ncbi.nlm.nih) with BioProject ID PRJNA793896.

2.3. Predicting target genes and identifying DEGs that are targets of miR-153

TargetScan 7.2 (version 7.2, http://www.targetscan.org) was used to screen the target genes of miR-153. Broadly conserved and confidentially annotated targets of miR-153-3p were used as reference (Supplementary 1). Subsequently, to explore the possible targets of miR-153 among the DEGs, the downregulated DEGs that were targets of miR-153 were identified in rLV-miR-153 cells using the Venn diagram webtool (http://bioinformatics.psb.ugent.be/webtools/Venn/).

2.4. Functional enrichment and pathway analysis

Gene Ontology (GO) annotation and Kyoto Encyclopedia of Genes and Genomes (KEGG) pathway enrichment analyses were used to analyze the functions of DEGs, and the intersection of miR-153 targets and DEGs. The Database for Annotation, Visualization and Integrated Discovery (DAVID; version 6.8, https://david.ncifcrf.gov/) was used to perform mRNA DEG enrichment analysis. $P < 0.05$ was considered statistically significant.

2.5. Construction of protein-protein interaction (PPI) networks and identification of hub genes

The Search Tool for the Retrieval of Interacting Genes (STRING, version 11.5) was used to construct a PPI network for the DEGs. Two groups of genes (down-regulated and up-regulated DEGs) were entered separately into the STRING database for further analysis. PPI node pairs with an interaction score of >0.4 (medium confidence) were selected. The PPI network was visualized using Cytoscape software (version 3.7.2, https://cytoscape.org/) with the node pairs and attributes of the nodes obtained from PPI analysis. MCODE, a plugin in Cytoscape, was used to identify hub genes, with a maximum depth of 100, a node score cutoff of 0.2, and a k-core of 2.

2.6. Gene Set Enrichment Analysis (GSEA)

GSEA is a computational approach used to determine whether members of a given gene set are enriched among the most differentially expressed genes between two biological states. The local version of the GSEA analysis tool (http://www.broadinstitute.org/gsea/index.jsp) was used to perform GSEA on the GO and KEGG datasets. In this study, GSEA was performed to identify gene sets enriched in rLV-miR-153 cells relative to the rLV-miR control. Gene sets were considered significantly enriched if their false discovery rate (FDR) q-value was <0.25, the NOM-p value < 0.05 and $|NES| > 1$.

2.7. RNA extraction, reverse transcription (RT) and qPCR

Total RNA was purified using the TRIzol reagent (Takara). RT was performed using 5X Primescript RT Master Mix (Takara), and cDNA samples were analyzed using qPCR (SuperReal SYBR Green PreMix Plus, FP205, Tiangen Biotech Co., Ltd.) with primers of mouse origin. For qPCR, 10 ng of RNA was used for each test, and the reactions were performed in triplicate on a StepOnePlus thermocycler (Applied Biosystems; Thermo Fisher Scientific, Inc.). The data were normalized against the levels of β-actin mRNA. The primers were as follows: Cdh5: forward, 5′-CAGCAACTTCACCCTCATAAAC-3′ and reverse, 5′-TCCCGATTAAACTGCCCATAC-3’; Nrcam: forward, 5′-CCCTGATTCTCTTCCTGTGC-3′ and reverse, 5′-TGAGTGATGGTTGGAGGTTG-3’; P2rx4: forward, 5′-AATTGGGACTGGAAGGTGTG-3′ and reverse, 5′-CAAGAGGGTGAAGTTTTCTGC-3’; Bdnf: forward, 5′-GTGACAGTATTAGCGAGTGGG-3′ and reverse, 5′-GGGATTACACTTGGTCTCGTAG-3’; Ntrk2: forward, 5′-GAACGAGTATGGGAAGGATGAG-3′ and reverse, 5′-AGGACTTCAGGGTAATTTGGG-3’; Kcnc3: forward, 5′-GTGATTGAAACCAACAGGGC-3′ and reverse, 5′-AGTGATTGGGCTCTTGTCTTC-3’; Kcna4: forward, 5′-CCCATTTCCAAAGCATTCCAG-3′ and reverse, 5′-GACCCCACAATCTTTCCCC-3’; Scn5a: forward, 5′-ACATGACAGCCGAGTTTGAG-3′ and reverse, 5′-GTCGAAGATATTCCAGCCCTG-3’; Grik3: forward, 5′-CGAGAAGGTTGGAGTATGGAG-3′ and reverse, 5′-CTTGCGGAACATGACAAAAGG-3’; β-actin: forward, 5′-GAGGTATCCTGACCCTGAAGTA-3′ and reverse: 5′-GCTCGAAGTCTAGAGCAACATAG-3’.

2.8. Expression profile of hub genes and DEGs that are targets of miR-153

The Gene Expression Omnibus (GEO) Profiles database (https://www.ncbi.nlm.nih.gov/geoprofiles/) contains gene expression profiles derived from curated GEO DataSets. Some of the identified hub and down regulated genes that were targets of miR-153 in this study were also searched within the GEO Profiles. GDS3442 contains 16 mouse brain samples on E9.5 (six samples), E11.5 (four samples) and E13.5 (six samples). The expression profiles of genes, including Cdh5, Nrcam, P2rx4, Ntrk2, Kcnc3, and Clcn5, which were identified in this study, across 12 samples at E9.5 and E13.5, in the GDS3442 dataset were selected and further analyzed. Data processing was performed using the Array-Pro Analyzer software (version 4.5, Media Cybernetics). The expression value of Cdh5 (https://www.ncbi.nlm.nih.gov/geoprofiles/65839962), Nrcam (https://www.ncbi.nlm.nih.gov/geoprofiles/65836589), P2rx4 (https://www.ncbi.nlm.nih.gov/geoprofiles/65831531), Ntrk2 (https://www.ncbi.nlm.nih.gov/geoprofiles/65841311), Kcnc3 (https://www.ncbi.nlm.nih.gov/geoprofiles/65827987) and Clcn5 (https://www.ncbi.nlm.nih.gov/geoprofiles/65856782) were all from GDS3442 and downloaded from the GEO Profiles and compared between E9.5 and E13.5.

2.9. Analysis of cell viability

Cell viability was determined using a CCK8 assay (Signalway Antibody Co.; Lot 8620). In untreated group, rLV-miR and rLV-miR-153 cells were cultured in 96-well plates ($1x10^3$ cells per well). Aβ peptide (1–42) human (P9001) and Aβ peptide (42-1) human (P9005) were purchased from Beyotime Biotechnology (Shanghai, China) and dissolved in distilled water. In the Aβ-treated group, rLV-miR and rLV-miR-153 cells were first treated with 100 μM $Aβ_{1-42}$, and in the control group, rLV-miR and rLV-miR-153 cells were treated with 100 μM $Aβ_{42-1}$. After incubating for 48 h, the Aβ treated cells of rLV-miR and rLV-miR-153 were further cultured in 96-well plates ($1x10^3$ cells per well) without Aβ treatment. After incubation for 0–4 days, both untreated and Aβ-treated groups of cells were

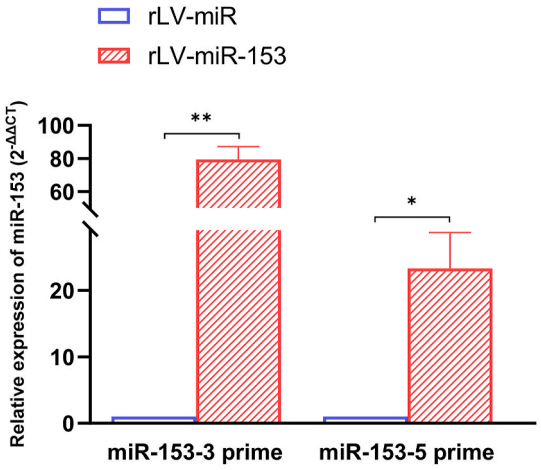

Fig. 2. Identification of the expression of mature mmu miR-153 in HT-22 cells by qPCR analysis. The relative expression of mature mmu miR-153-3 prime (MIMAT0000163) and mmu miR-153-5 prime (MIMAT0016992) is shown. Relative expression was calculated using the relative cycle quantification method ($2^{-\Delta\Delta Ct}$) and normalized to U6. Significance was determined by comparing rLV-miR-153 to rLV-miR control with two-tailed student's t-test. Error bars represent standard deviation. *P < 0.05, **P < 0.01.

incubated with CCK8 (10 μL CCK8 was added to each well) for 1 h at 37 °C. Absorbance was measured at 450 nm using a SpetraMax M3 (Molecular Devices, LLC).

2.10. Statistical analysis

Statistical significance in CCK8 assay was determined using ANOVA and multiple comparison, and qPCR and GEO profiles were compared by Student's t-test using GraphPad Prism (version 7.0, GraphPad Software, Inc.). Statistical significance was set at $p < 0.05$.

3. Results

3.1. Identification of miR-153 expression in HT-22 stable cell lines

As shown as in Fig. 2, the qPCR result demonstrated that both mature miR-153-3 prime and mature miR-153-5 prime were significantly increased in rLV-miR-153 cells compared with those in the rLV-miR control cells (miR-153-3 prime: 79.2851 ± 7.8484 vs. 1.0000 ± 0.0000, $p = 0.0033$; and miR-153-5 prime: 23.2576 ± 5.4276 vs. 1.0000 ± 0.0000, $p = 0.0192$). These results suggested that mature mmu miR-153 overexpressing HT-22 stable cell lines were suitable for further analyses.

3.2. RNA-sequencing and differential expression analysis

To identify the molecules and signaling pathways in miR-153 overexpressed HT-22 cells, RNA-sequencing was performed to obtain an overview of the changes in gene expression. Six cDNA libraries were prepared for sequencing, including three replicates of the control rLV-miR and rLV-miR-153 cells. The total mapping rates between clean reads and the reference genome were approximately 92.27 % and 88.93 % for the rLV-miR and rLV-miR-153 cells, respectively. Differential expression analysis indicated that there were 2524 differentially expressed genes in rLV-miR-153 cells compared with those in rLV-miR cells. Among them, 1649 genes were up regulated and 875 genes were down regulated (Supplementary 2). The target genes of miR-153 were predicted using TargetScan 7.2. In total, 709 target genes (Supplementary 1) and 29 DEGs were identified as miR-153 targets using the Venn diagram webtool. RNA sequencing provide an overview of changes in mRNA expression caused by miR-153 overexpression. Based on RNA sequencing, we further extracted and analyzed theses data to identify the possible molecular mechanisms underlying the effects of miR-153.

Table 1
GO terms of differentially expressed genes (DEGs).

Category	GO terms	Number of genes	P value	DEGs
BP	GO:0007155~cell adhesion	54	4.29E-06	Up-regulated DEGs
	GO:0007169~transmembrane receptor protein tyrosine kinase signaling pathway	18	4.73E-05	
	GO:0009408~response to heat	13	7.28E-05	
	GO:0010976~positive regulation of neuron projection development	20	3.19E-04	
	GO:0019227~neuronal action potential propagation	4	0.0084	
	GO:0030182~neuron differentiation	15	0.0136	
	GO:0006260~DNA replication	18	6.50E-07	Down-regulated DEGs
	GO:0007275~multicellular organism development	61	1.54E-05	
	GO:0007067~mitotic nuclear division	24	5.44E-05	
CC	GO:0016020~membrane	514	2.93E-13	Up-regulated DEGs
	GO:0005887~integral component of plasma membrane	109	5.47E-08	
	GO:0009986~cell surface	68	5.90E-07	
	GO:0031410~cytoplasmic vesicle	55	0.0032	
	GO:0043025~neuronal cell body	46	0.0059	
	GO:0043005~neuron projection	36	0.0160	
	GO:0043197~dendritic spine	16	0.0217	
	GO:0045202~synapse	40	0.0350	
	GO:0097060~synaptic membrane	6	0.0374	
	GO:0005578~proteinaceous extracellular matrix	34	4.37E-09	Down- regulated DEGs
	GO:0005604~basement membrane	13	7.50E-05	
	GO:0005615~extracellular space	75	2.53E-04	
MF	GO:0005102~receptor binding	48	6.70E-06	Up-regulated DEGs
	GO:0005516~calmodulin binding	26	5.11E-05	
	GO:0005509~calcium ion binding	65	1.83E-04	
	GO:0004714~transmembrane receptor protein tyrosine kinase activity	12	2.23E-04	
	GO:0045296~cadherin binding	8	0.0011	
	GO:0050840~extracellular matrix binding	9	2.27E-06	Down- regulated DEGs
	GO:0005201~extracellular matrix structural constituent	8	3.42E-04	
	GO:0003697~single-stranded DNA binding	10	0.0016	

3.3. Functional enrichment and pathway analysis of the DEGs

Further enrichment analyses will contribute to elucidating the functions and pathways enriched in rLV-miR-153 cells. GO function enrichment analysis was first performed on the DEGs and the DEGs that were targets of miR-153. GO describes the knowledge of the biological domain with respect to three aspects: biological process (BP), cellular component (CC), and molecular function (MF). The upregulated and downregulated genes were analyzed separately using the DAVID database, and the analysis of DEGs between rLV-miR-153 and rLV-miR cells is shown in Table 1. In the BP-based GO terms, the upregulated DEGs were mainly enriched in cell adhesion, receptor protein tyrosine kinase signaling (RTK), neuron projection development, and differentiation, whereas the downregulated DEGs were mainly enriched in DNA replication. In the CC-based GO terms, the upregulated DEGs were mainly distributed in the cell membrane and neuron projection, while the downregulated DEGs were mainly enriched in the basement membrane and extracellular space. In the MF-based GO terms, the upregulated DEGs were mainly enriched in receptor binding, including calmodulin, calcium ion, and cadherin binding; RTK activity was also increased. The downregulated DEGs were mainly enriched in the extracellular matrix and single-stranded DNA binding. As shown in Fig. 3 of the KEGG analysis, similar to the GO function analysis of upregulated DEGs, the cell adhesion and calcium signaling pathways were significantly increased in miR-153 cells. For the downregulated DEGs, the pathway was also focused on DNA replication (Fig. 3), which was consistent with the GO function analysis (Table 1).

GO function and pathway analysis results indicated that miR-153 increased cell adhesion, neurite outgrowth, and synapse function-related functional pathways while attenuating cell proliferation in HT-22 cells, which may affect the neuronal differentiation process.

3.4. Construction of PPI networks and identification of hub genes in upregulated DEGs

To identify hub genes, PPI networks were constructed using upregulated DEGs in significantly altered GO functions, including BP, CC and MF (Table 1). As shown in Fig. 4A, the PPI network constructed for the BP of the GO functions exhibited 112 nodes and 278 edges. MCODE analysis identified seven clusters (Fig. 4B), including 40 hub genes: Flt4, Cdh5, Itga2b, Col18a1, Erbb3, Il6, Pdgfrb, Hspa1b, Itga6, and Cd34 (cluster 1); Itgb4, Itga7, Lyn, Col7a1, Lamb3, and Lama4 (cluster 2); Wnt10b, Wnt6, Wnt9a, and Wnt10a (cluster 3); Asic3, Trpv3, Calca, and P2rx3 (cluster 4); Ctnnd2, Cdh26, Insrr, and Cdh13 (cluster 5); Itgb2, Tyk2, Lif, Madcam1, Osm, Shc2, Sele, Selp, and Sspo (cluster 6); Scn1a, Nrcam, and Scn1b (cluster 7).

As shown in Fig. 5A, the PPI network constructed for the CC of GO functions contained 572 nodes and 1537 edges. MCODE analysis identified 16 clusters (Fig. 5B), including 152 hub genes: Il33, Nrros, Ncf2, Ly6c1, Ly6c2, Il12b, Cd274, Cd27, Il7r, Itgb4, Nckap1l, Pld4, Laptm5, Tspan32, Cd40, Fcgr2b, Lyn, Tyrobp, and Coro1a (cluster 1); Igtp, Irgm2, Gbp4, Oasl1, and Ifi203 (cluster 2); Adra2b, Arhgef28, Grid2ip, Adcy3, Rnd1, Gna15, Fmn2, Gng3, Rhod, and Adcy9 (cluster 3); B3galt5, B4galnt1, St3gal3, B4galt2, C1galt1, Gcnt2, and Galnt3 (cluster 4); Nod1, Nod2, Sdc4, Plcg2, Flt4, Itga6, Pdgfrb, Cd209a, Slc15a3, Cd74, Cat, Cd83, Atf6, Tnfsf13b, Hmox1, Notch3, Tlr3, Casp4, Sqstm1, Cdh5, Tgfbr2, Bid, and Naip1 (cluster 5); Itga7, Procr, Vegfc, Vcan, Lck, Dsel, Chst3, Ly6a, Itga2b, Selp, H2-Q1, H2-Q4, F3, Csgalnact1, Reln, Chst14, Jag1, Msn, Myo7a, Sele, Ephb4, and Esam (cluster 6); Wnt6, Fzd4, Fzd9, Lrrtm4, Limk1, Rgs2, Dlg3, Dlg2, Gsk3b, Nos3, Rgs17, Nrcam, and Agtr1a (cluster 7); Madcam1, Capn1, Capn2, Myo6, Picalm, Itgb2, Epn3, Cd34, Grb14, Espn, Kcnmb2, Kcnj6, Specc1, Kcnu1, Erbb3, Myo1c, Kcnj4, Synj1, Fkbp1b, Kcnn2, Fgfr1, Kcnn1, and Tgfb1 (cluster 8); S1pr4, Sgpp2, and Sgpp1 (cluster 9); P2ry2, P2rx4, and P2rx16 (cluster 10); Abcb4, Cyp27a1, and Slco1a (cluster 11); Slc17a7, Ntrk2, and Gabrg2 (cluster 12); Kcnh3, Kcnk12, and Kcnk6 (cluster 13); Gpr75, Gpr85, and Gprc5b (cluster 14); Clca1, Clca2, and Ugt3a2 (cluster 15); Cnga3, Chn2, Slc22a21, Rhov, Slc16a9, Stard10, Unc93a, Gnb3, and Rhoq (cluster 16).

As shown in Fig. 6A, the PPI network constructed for the MF of GO functions exhibited 149 nodes and 254 edges. MCODE analysis identified six clusters (Fig. 6B), including 33 hub genes: H2-Q1, H2-M10.2, H2-Q4, H2-M10.3, and Tyrobp (cluster 1); Fgf9, Fgf15, Il6,

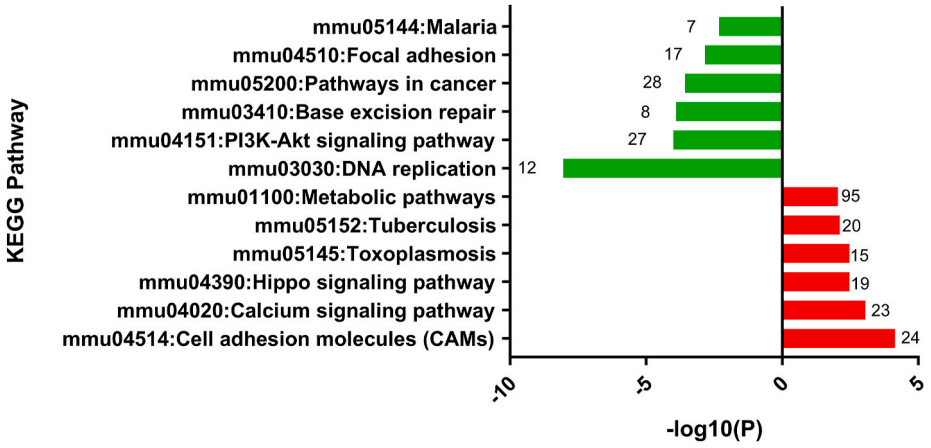

Fig. 3. Kyoto Encyclopedia of Genes and Genomes (KEGG) analysis of DEGs in rLV-miR-153 cells. Red column indicates the upregulated DEGs. Green column indicates the downregulated DEGs. The number beside each column indicated the number of genes involved in each pathway.

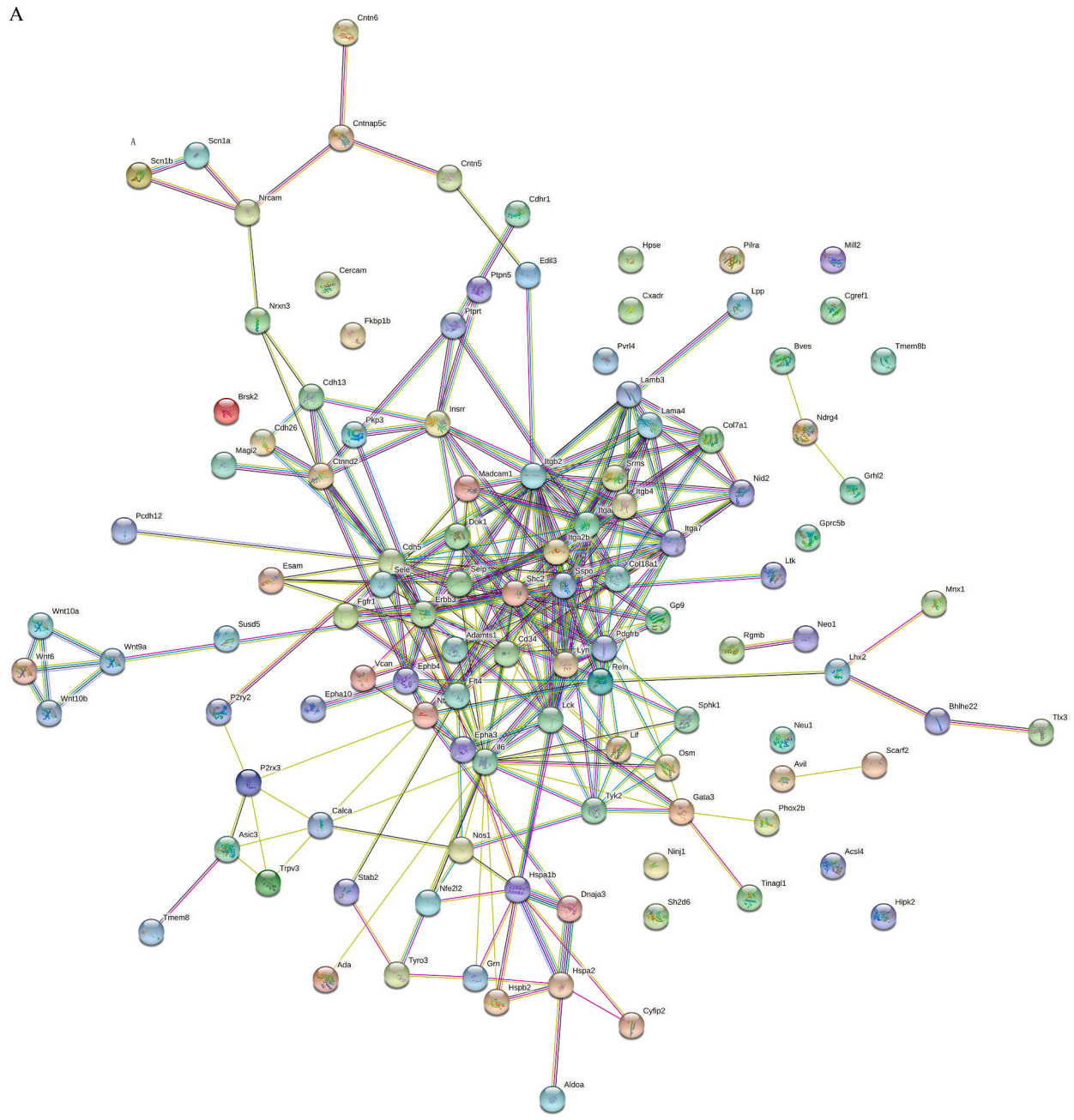

Fig. 4. Protein–protein interaction network for biological process (BP) of GO functions. **A.** The interaction network is between upregulated DEGs in rLV-miR-153 cells. **B**. The yellow rectangles represent the 40 hub genes identified in the 7 clusters of the network.

Fgfr3, and Ntrk2 (cluster 2); Jag1, Notch3, Ephb4, and Fgfr1 (cluster 3); Hmgcl, Msn, Acox2, Nos2, Sphk1, Lyn, Acot2, Ehhadh, Tyk2, and Nos3 (cluster 4); Wnt10b, Wnt6, and Wnt10a (cluster 5); Nos1, Erbb3, Sele, Cat, Flt4, and Cdh5 (cluster 6).

Among the hub genes, many molecules functioned in neural development. To determine the gene expression of hub genes, we selected several representative genes for further identification by qPCR. For example, the CaM/Calmodulin-related molecules, Cdh5, Nrcam and P2rx4. Cadherin 5 (Cdh5) was identified as a hub gene for BP (cluster 1), CC (cluster 5), and MF (cluster 6). Cdh5 was significantly higher in rLV-miR153 cells than that in the rLV-miR control (log2FC = 6.3436, p = 2.07E-61), as determined by RNA sequencing. Notably, Neuronal cell adhesion molecule (Nrcam), another hub gene in cluster 7 of both the BP and CC, was increased and localized in the synapse. Purinergic receptor P2X, ligand-gated ion channel 4 (P2rx4) was identified as a hub gene in cluster 11 of the CC and was localized to the membrane and synapse.

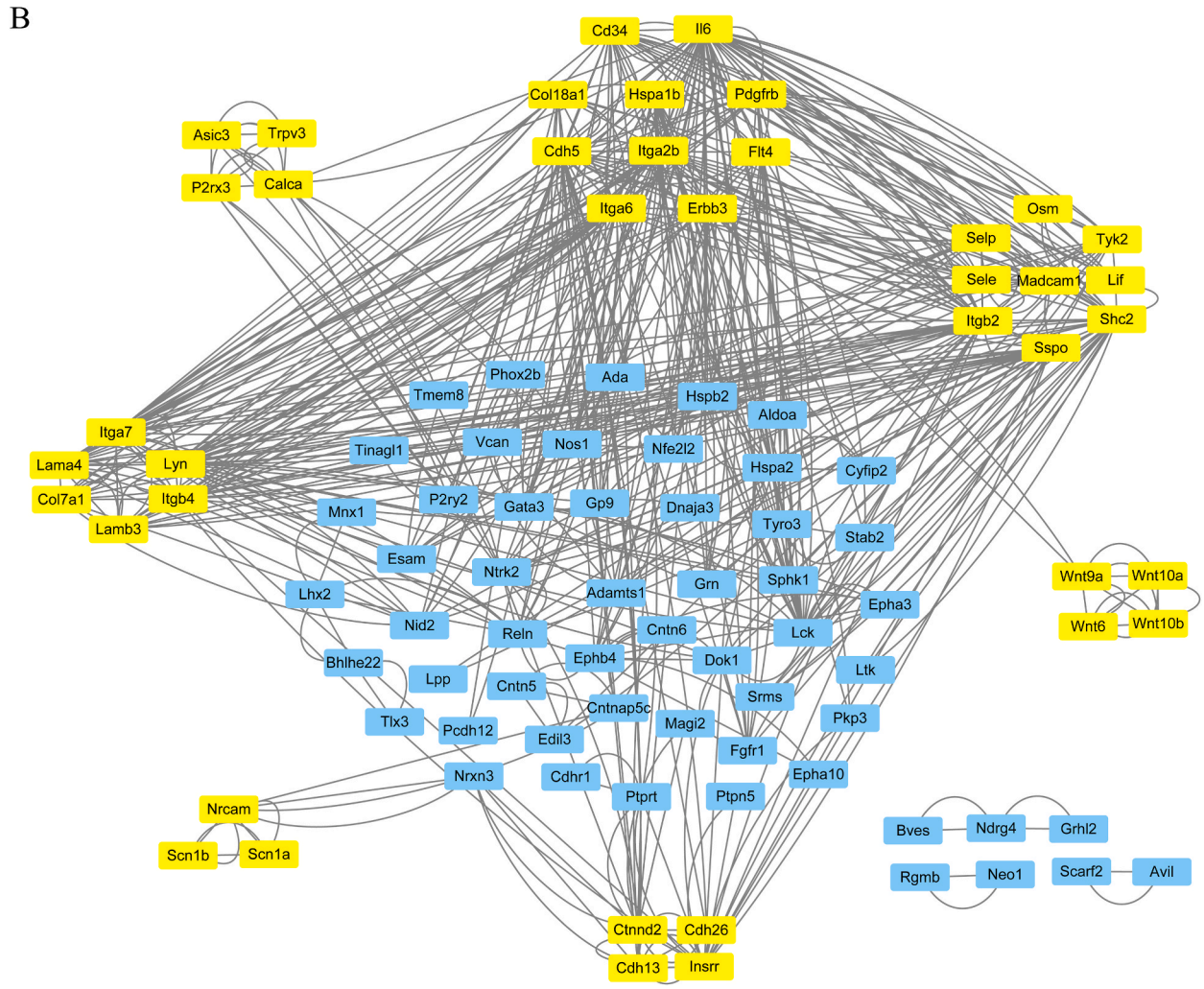

Fig. 4. (*continued*).

In addition, the transmembrane receptor protein tyrosine kinase signaling pathway was significantly clustered. It was noted that neurotrophic receptor tyrosine kinase 2 (Ntrk2) was identified as a hub gene in cluster 12 of CC and cluster 2 of MF. Ntrk2 was markedly increased in rLV-miR153 cells compared with the that in rLV-miR control (log2FC = 4.6116, p = 0.0094) by RNA sequencing and was localized in the membrane and dendritic spines. Notably, Brain derived neurotrophic factor (Bdnf) was increased in rLV-miR153 cells compared with that in the rLV-miR control (log2FC = 2.3824, p = 0.0192) by RNA sequencing. Therefore, Ntrk2 and Bdnf were selected for the subsequent qPCR analysis.

Taken together, Fig. 6 shows that most hub genes were involved in the cell adhesion, calmodulin/calcium binding, and RTK signaling pathway BPs, and may play a role in neuronal differentiation, axon growth, and synaptic function.

3.5. Ion-channel activity that is target of miR-153 was downregulated

To further explore the possible function of the target of miR-153, we performed GO function analysis on the downregulated genes that were targets of miR-153. As shown in Table 2, ion channel- and transport-related molecules were significantly downregulated in both BP and MF GO functions, especially potassium voltage-gated channel-related and sodium channel-voltage-gated related genes such as Kcnc3, Kcna4 and Scn5a, which are involved in multiple GO terms. In addition, the chloride channels of Clcn5 and the glutamate receptor of Grik3 decreased and clustered in the downregulated ion channel activity.

Ion channel species and membrane potential of neural progenitor cells (NPCs) change during neural differentiation [13]. Down-regulation of ion channel expression may help to regulate the electrophysiological maturity of rLV-miR153 cells.

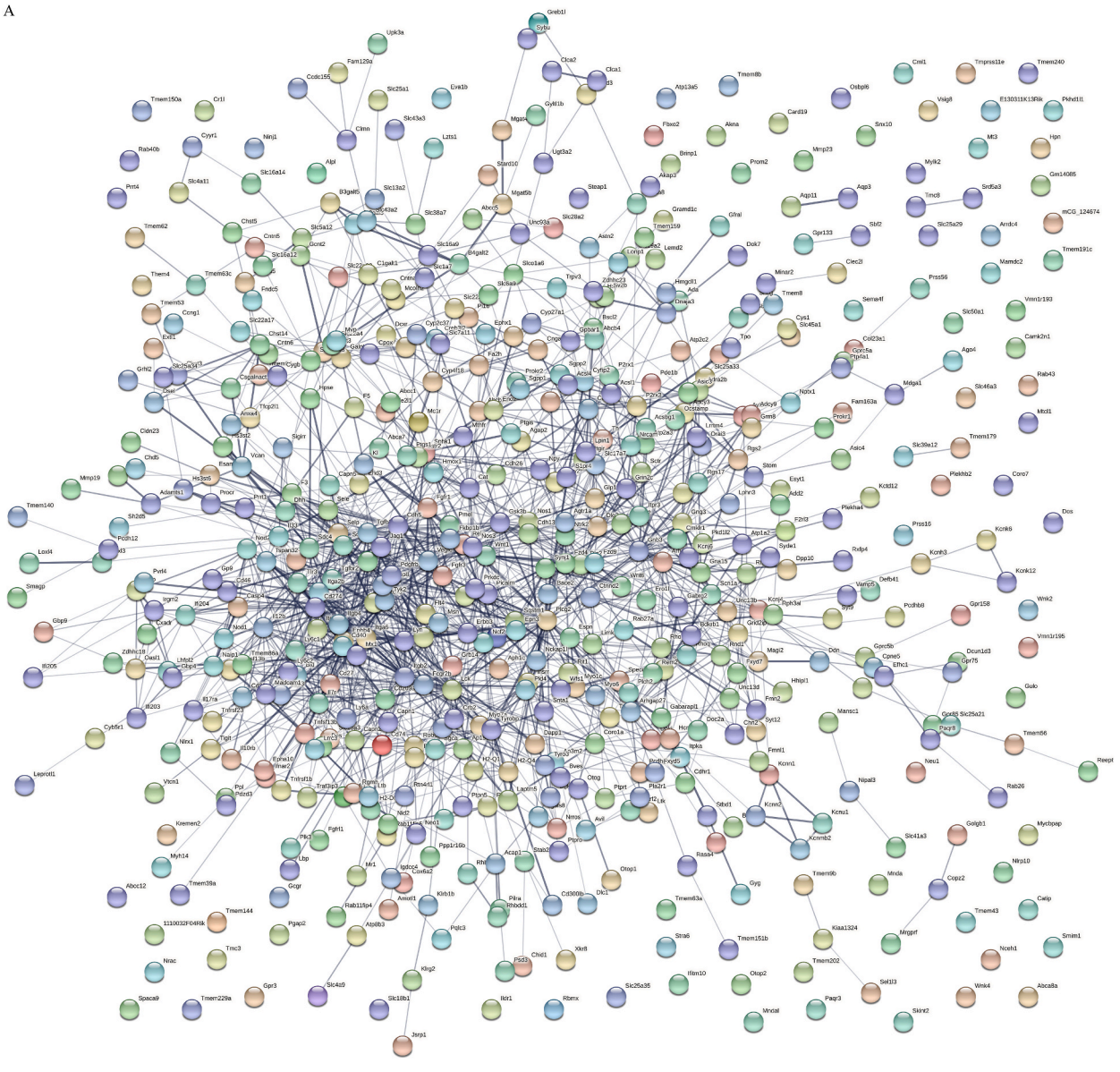

Fig. 5. Protein–protein interaction network for cellular components (CC) of GO functions. **A.** The interaction network is between upregulated DEGs in rLV-miR-153 cells. **B.** The yellow rectangles represent the 152 hub genes identified in the 16 clusters of the network.

B

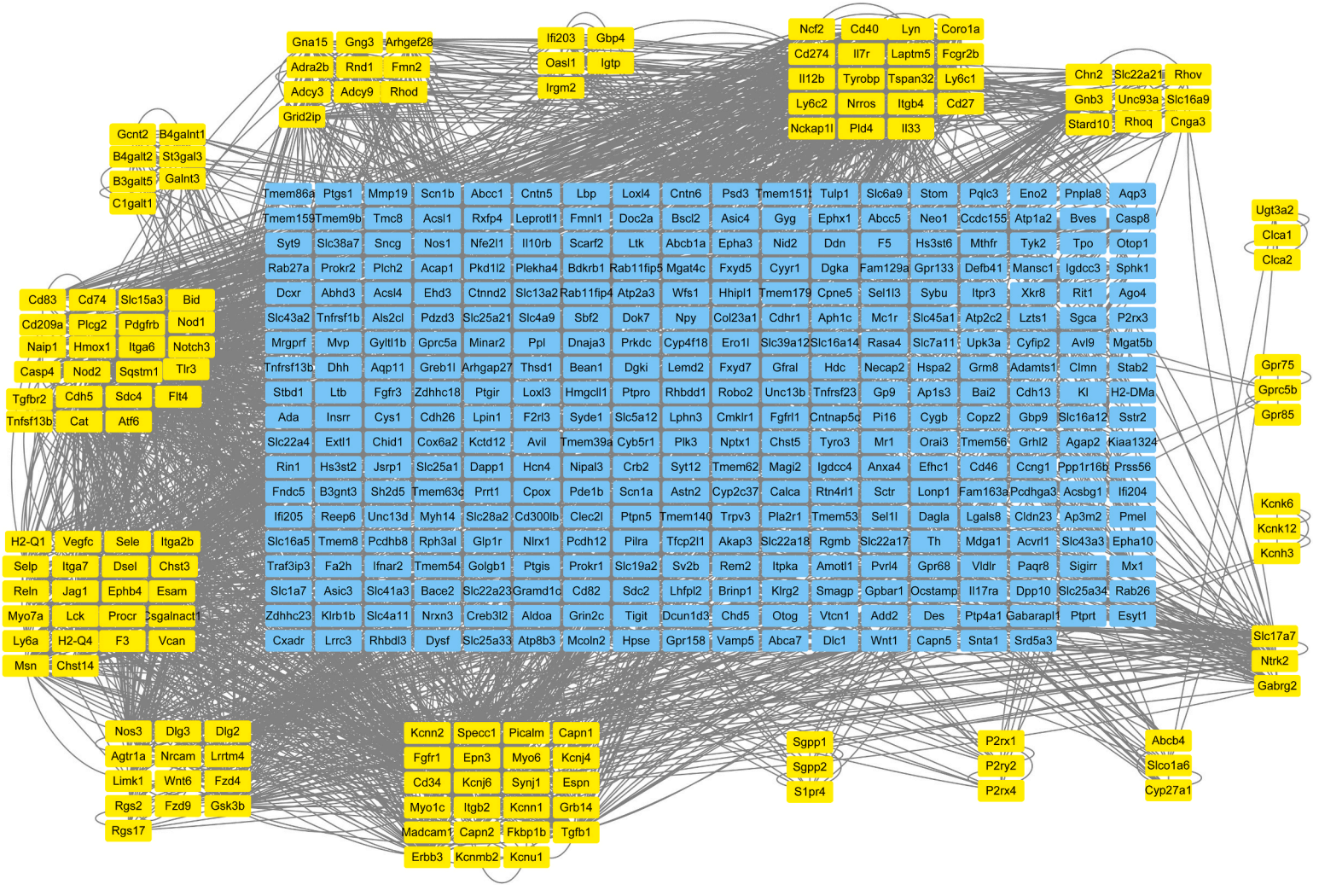

Fig. 5. (*continued*).

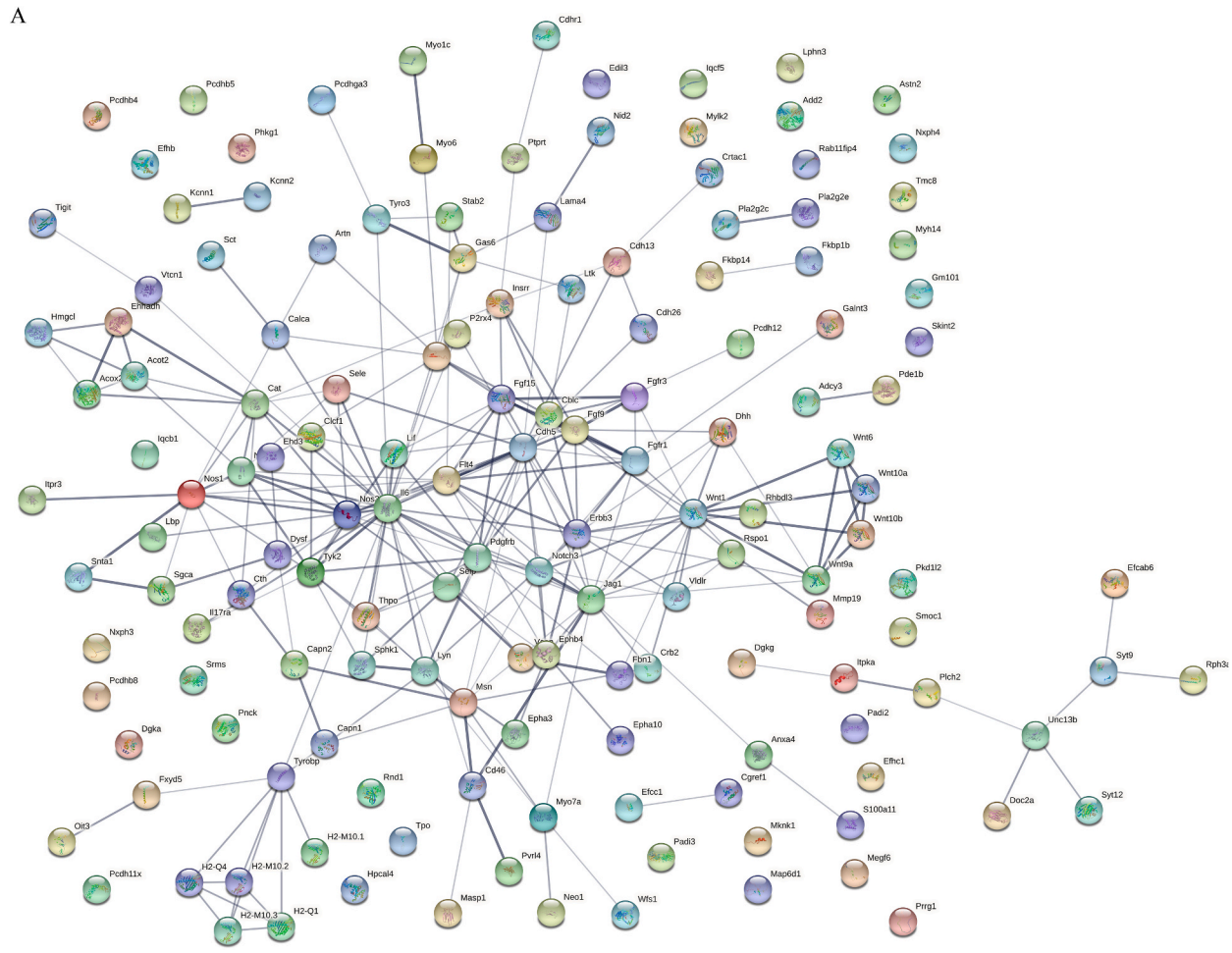

Fig. 6. Protein–protein interaction network for molecular function (MF) of GO functions. **A.** The interaction network is between upregulated DEGs in rLV-miR-153 cells. **B**. The yellow rectangles represent the 33 hub genes identified in the 6 clusters of the network.

3.6. Hub genes increased and ion channel genes decreased in mRNA level by qPCR analysis

Based on the above enrichment analysis results, we detected the expression of representative genes by qPCR. The upregulated genes included Cdh5, Nrcam, P2rx4, Ntrk2, and Bdnf. As shown as in Fig. 7A, cell adhesion/Ca^{2+} signaling related molecules of Cdh5 (58.2027 ± 13.7128 vs. 1.0000 ± 0.0000, p = 0.0186), Nrcam (7.3692 ± 3.1192 vs. 1.0000 ± 0.0000, p = 0.0241), and P2rx4 (2.4857 ± 0.0534 vs. 1.0000 ± 0.0000, p = 0.0004) increased significantly in rLV-miR-153 cells compared with those in the rLV-miR control. Furthermore, for RTK signaling-related molecules, both Bdnf (6.2761 ± 0.9399 vs. 1.0000 ± 0.0000, p = 0.0104) and Ntrk2 (11.7148 ± 4.6055 vs. 1.0000 ± 0.0000, p = 0.0157) also substantially increased in rLV-miR-153 cells compared with those in the rLV-miR control.

Down-regulated ion channel-related genes were also detected. As indicated in Fig. 7B, Kcnc3 (0.7753 ± 0.0510 vs. 1.0000 ± 0.0000, p = 0.0168), Kcna4 (0.4726 ± 0.0629 vs. 1.0000 ± 0.0000, p = 0.0047), Scn5a (0.1628 ± 0.0407 vs. 1.0000 ± 0.0000, p = 0.0008) and Grik3 (0.0672 ± 0.0525 vs. 1.0000 ± 0.0000, p = 0.0011) were significantly down regulated in rLV-miR153 cells compared with those in the rLV-miR control. The results of qPCR helped to confirm the change in the expression of cell adhesion and ion channel-related hub genes identified in the enrichment analysis.

3.7. GSEA indicated the consistent function cluster with differential expression analysis

GSEA can include subtle expression changes between two biological groups without a pre-defined threshold for differential expressed genes. GSEA indicated that gene sets, including CADHERIN BINDING (GO:0045296) (Fig. 8A), and LIGAND-GATED CALCIUM CHANNEL ACTIVITY(GO:0099604) (Fig. 8B) were positively correlated in rLV-miR-153 cells. Notably, the PHOSPHATIDYLINOSITOL PHOSPHOLIPASE C ACTIVITY (GO:0004435) (Fig. 8C) and PHOSPHOLIPASE C ACTIVITY (GO:0004629) (Fig. 8D) gene sets

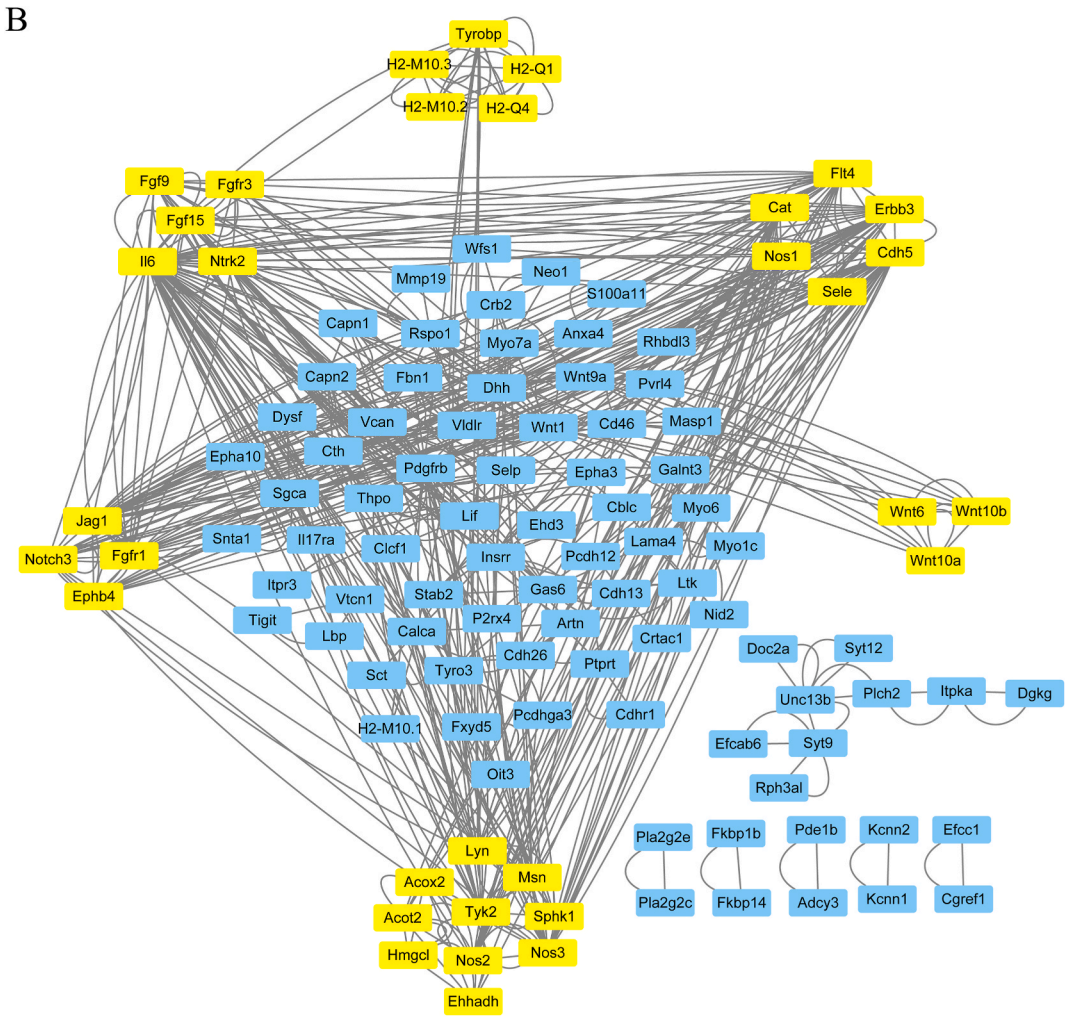

Fig. 6. (*continued*).

Table 2
GO terms of down regulated genes that are targets of miR-153.

Category	GO terms (gene symbol)	Number of genes	P value	DEGs
BP	**GO:0071805~potassium ion transmembrane transport** (Slc9a6, Kcnc3, Kcna4)	3	0.0079	Down-regulated
	GO:0006811~ion transport (Clcn5, Kcnc3, Grik3, Kcna4, Scn5a)	5	0.0105	DEGs
	GO:0055085~transmembrane transport (Clcn5, Kcnc3, Kcna4, Scn5a)	4	0.0165	
	GO:0034765~regulation of ion transmembrane transport (Kcnc3, Kcna4, Scn5a)	3	0.0172	
CC	**GO:0045177~apical part of cell** (Clcn5, Fzd3, Dab1)	3	0.0116	Down-regulated
	GO:0030424~axon (Nfasc, Fzd3, Grik3, Kcna4)	4	0.0153	DEGs
MF	**GO:0005216~ion channel activity** (Clcn5, Kcnc3, Grik3, Kcna4, Scn5a)	5	1.48E-04	Down- regulated DEGs
	GO:0005515~protein binding (Fzd3, Aust2, Grik3, Unc5c, Nrep, Lamc1, Runx2, Bach2, Adam19, Nfasc, Dab1, Myb, Six3, Scn5a, Lhx9)	15	0.0020	
	GO:0005244~voltage-gated ion channel activity (Kcnc3, Kcna4, Scn5a)	3	0.0194	

were also clustered and positively correlated in rLV-miR-153 cells, which may mediate the signal transduction downstream of both calcium signaling and the Bdnf/Nrtk2 pathway. Notably, Cdh5 and P2rx4 contributed to the core enrichment of CADHERIN BINDING (GO:0045296), and P2rx4 also contributed to the core enrichment of LIGAND-GATED CALCIUM CHANNEL ACTIVITY (GO:0099604). Moreover, TRANSMITTER-GATED CHANNEL ACTIVITY (GO:0022835) (Fig. 8E) and TRANSMITTER-GATED ION CHANNEL ACTIVITY (GO:0022824) (Fig. 8F) were the top two gene sets that were negatively correlated in rLV-miR-153 cells, consistent with the GO function of the down regulated genes that are targets of miR-153 (Table 2). One of the identified target genes—Grik3 was among the

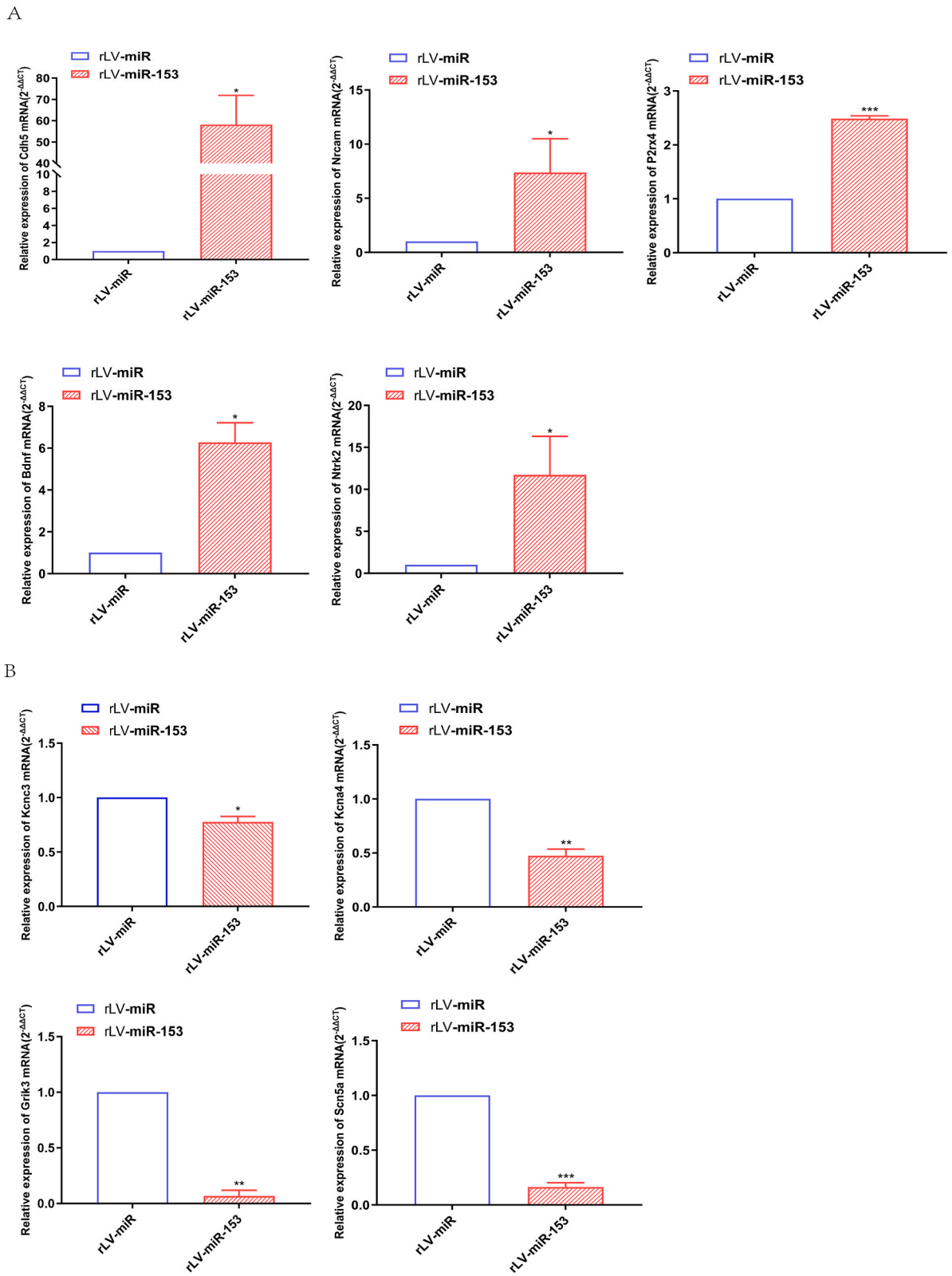

Fig. 7. q-PCR analysis of selectively representative genes. **A.** Cell adhesion/Ca^{2+} signaling related genes of Cdh5, Nrcam and P2rx4; RTK signaling related genes of Bdnf and Ntrk2. **B**. Ion channel related genes of Kcnc3, Kcna4, Grik3 and Scn5a. β-Actin was used as an internal control. Data are given as mean ± SD (n = 3). Error bars represent SD. *p < 0.05; **p < 0.01; ***p < 0.001.

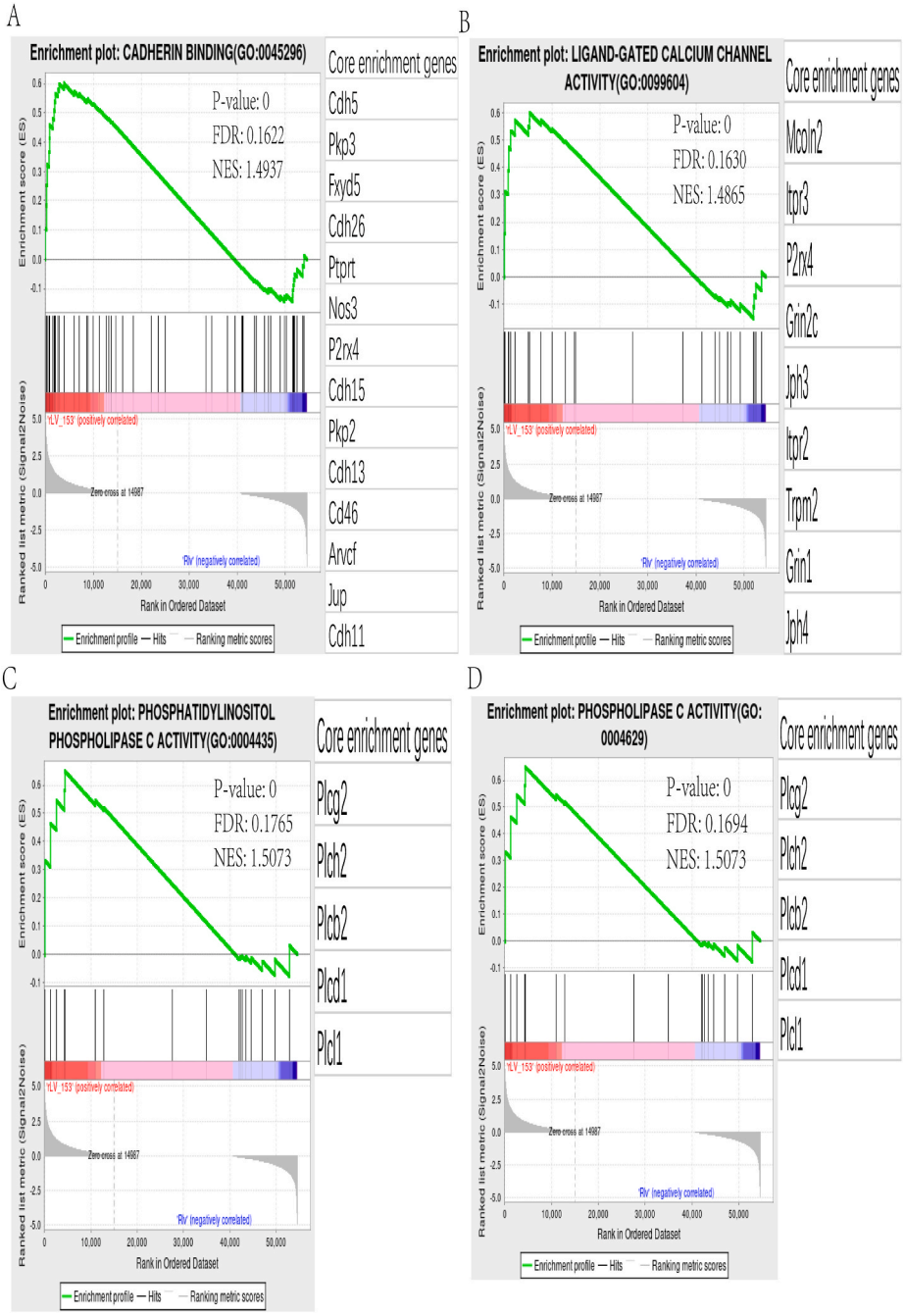

Fig. 8. Gene set enrichment analysis on GO function and KEGG between rLV-miR-153 and rLV-miR cells. **A-F**: GSEA enrichment plot on GO function. **G**: GSEA enrichment plot on KEGG. NES = normalized enrichment score. Core genes that contribute to the enrichment are in the listbox beside each enrichment plot.

core enrichment genes in both TRANSMITTER-GATED CHANNEL ACTIVITY (GO:0022835) and TRANSMITTER-GATED ION CHANNEL ACTIVITY(GO:0022824). Similarly, KEGG GSEA indicated that the gene set of CELL ADHESION MOLECULES (CAMS) (MMU04514) (Fig. 8G) was also positively correlated with rLV-miR-153 cells.

Both GSEA and GO were used for enrichment analysis to ensure functional and pathway change in rLV-miR-153 cells. GSEA showed that the cell adhesion/Ca^{2+} pathway was significantly clustered in rLV-miR-153 cells compared with that in rLV-miR control cells, which was consistent with the GO function analysis of DEGs (Table 1). Notably, significantly decreased ion channel activity was also

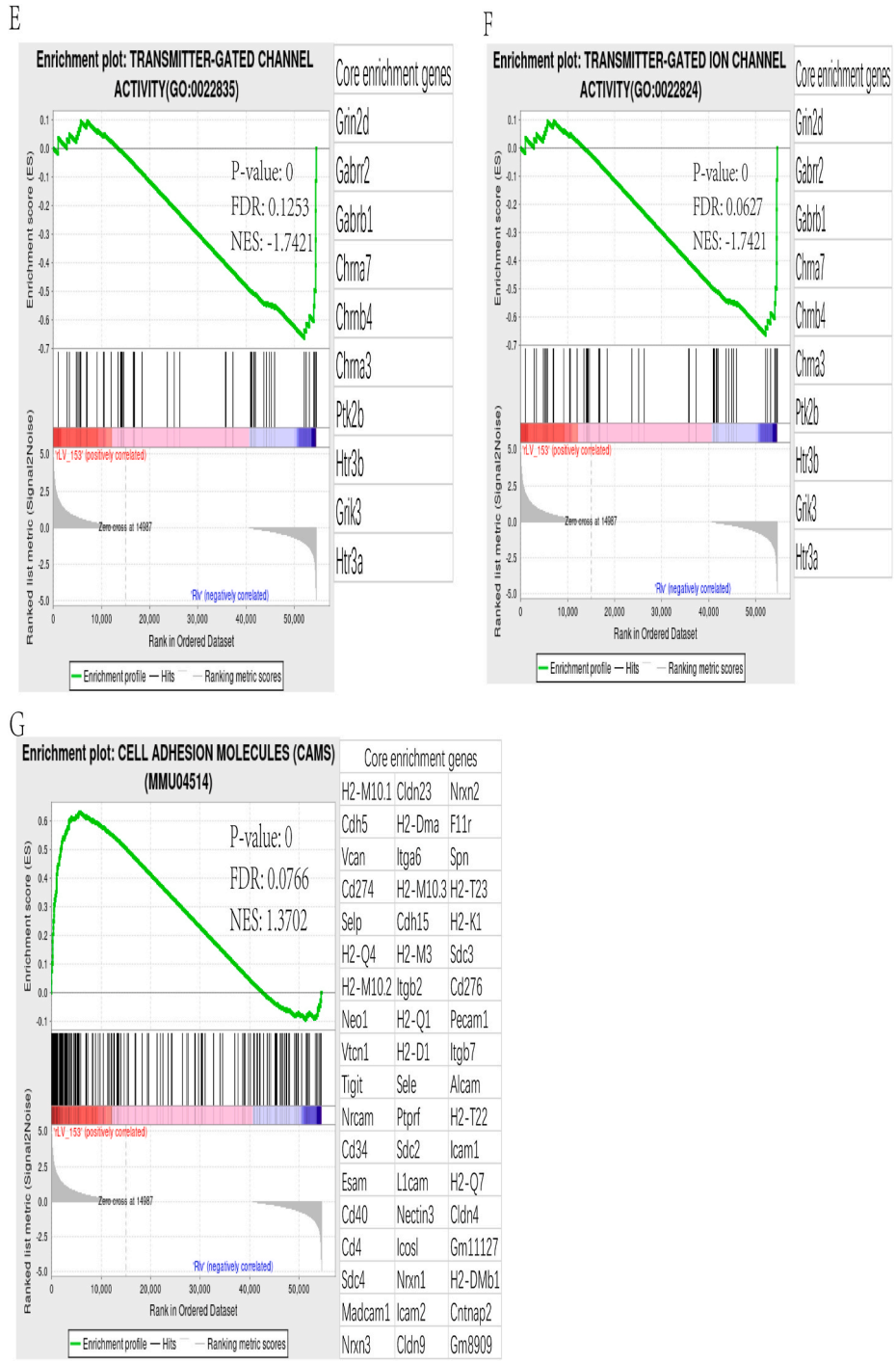

Fig. 8. (*continued*).

indicated in the GSEA analysis of rLV-miR-153 cells, which was consistent with the GO function analysis on the DEGs that were targets of miR-153 (Table 2).

3.8. Expression profile of the identified genes in GDS3442

The GDS3442 dataset is from the transcriptome and proteome analysis of early embryonic mouse brain development and indicates the expression changes between the time points E9.5, E11.5, and E13.5 [14]. To further compare the expression changes of the

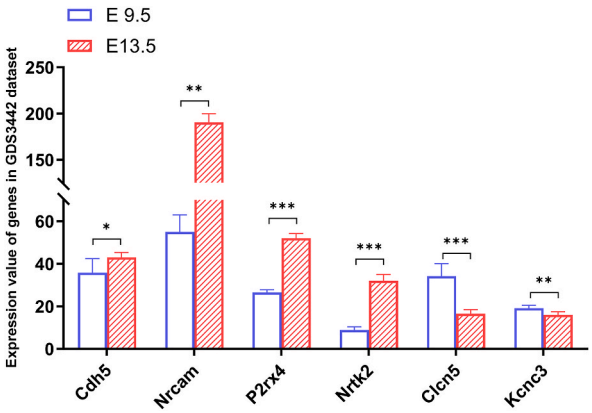

Fig. 9. Expression of hub genes and DEGs that are targets of miR-153.The expression profile of Cdh5, Nrcam, P2rx4, Ntrk2, Clcn5 and Kcnc3 in GDS3442 dataset of mouse embryonic brain was compared between E9.5 and E13.5. Data is represented as mean ± SD. n = 12. Error bars represent SD. *p < 0.05, **p < 0.01, ***p < 0.001.

identified genes in this study between the undifferentiated and differentiated stages, we selected the two time points, E9.5 (six samples) at the undifferentiated stage and E13.5 (six samples) at the differentiation peak in GDS3442 to perform the comparison. Based on the expression profile in the GDS3442 dataset, the expression profile of Cdh5 (43.0000 ± 2.3664 vs. 35.8333 ± 6.6156, p = 0.0450), Nrcam (190.5000 ± 9.1378 vs. 55.0000 ± 7.9750, p = 1.34E-10), P2rx4 (52.0000 ± 2.2804 vs. 26.5000 ± 1.3784, p = 8.01E-09), and Ntrk2 (32.0000 ± 2.9665 vs. 8.8333 ± 1.6021, p = 2.42E-07), which were identified as upregulated hub genes in this study, were found to be also upregulated in E13.5 samples compared with those in E9.5 samples (Fig. 9). Moreover, the expression profile of Kcnc3 (16.0000 ± 1.5492 vs. 19.1667 ± 1.3292, p = 0.0036) and Clcn5 (16.5000 ± 1.9748 vs. 34.1667 ± 5.9805, p = 0.0004), which were down regulated genes and targets of miR-153, were also downregulated in E13.5 samples compared with that in E9.5 samples (Fig. 9).

This suggests that neural cell adhesion and ion channel-related genes induced by miR-153 in rLV-miR-153 cells indicate a consistent change in gene expression during early embryonic mouse brain development.

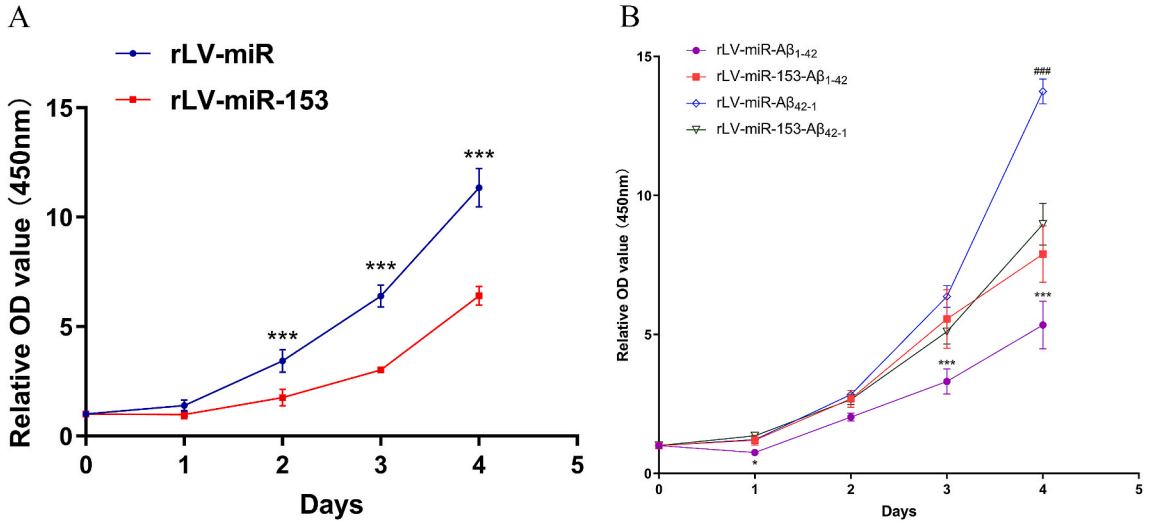

Fig. 10. **A**. Cell proliferation in the rLV-miR-153 and rLV-miR cells. CCK-8 is used to assay cell proliferation. Data are given as mean ± standard deviation (SD) (n = 3). Error bars represent SD. ***p < 0.001.**B**. Cell proliferation assay using CCK-8 in the rLV-miR and rLV-miR-153 groups. $A\beta_{1\text{-}42}$ treated group was pretreated by $A\beta_{1\text{-}42}$ peptide for 48 h, and was further cultured from 0 to 4 days respectively before performing CCK-8 assay, and $A\beta_{42\text{-}1}$ treatment was used as control. Data are given as mean ± standard deviation (SD) (n = 3). Error bars represent SD. ***/###p < 0.001. *** Statistical significance was between rLV-miR-153- $A\beta_{1\text{-}42}$ and rLV-miR- $A\beta_{1\text{-}42}$ group. ### Statistical significance was between rLV-miR-153- $A\beta_{42\text{-}1}$ and rLV-miR- $A\beta_{42\text{-}1}$ group.

3.9. miR-153 decreases the susceptibility of HT-22 cells to Aβ toxicity

To confirm the cell proliferation rate of rLV-miR-153- and rLV-miR-transfected cells, CCK8 assay was performed on rLV-miR-153- and rLV-miR-transfected cells from 0 to 4 days. As shown in Fig. 10A, the number of HT-22 cells increased slowly in the rLV-miR-153 cells compared with that in the rLV-miR cells from day 1–4, which was significantly slower at day 2 (1.7617 ± 0.3784 vs 3.4373 ± 0.5175, $p = 0.0004$), day 3 (3.0229 ± 0.1310 vs 6.3981 ± 0.5007, $p < 0.0001$), and day 4 (6.4067 ± 0.4289 vs 11.3477 ± 0.8761, $p < 0.0001$). Cell proliferation was attenuated in rLV-miR-153 cells, which was consistent with GO function and pathway analysis results of downregulated DNA replication (Fig. 3 and Table 1). In addition, to observe whether neural differentiation promoted by miR-153 can affect cellular response to Aβ toxicity, CCK8 assay was also used to compare the cell viability between groups of rLV-miR-153 cells and rLV-miR cells treated with $A\beta_{1\text{-}42}$ and control $A\beta_{42\text{-}1}$. Different from the result shown in Fig. 10A, rLV-miR-153 cells treated with $A\beta_{1\text{-}42}$ grew faster significantly than rLV-miR cells treated with $A\beta_{1\text{-}42}$ in day 3 (5.5567 ± 1.0555 vs 3.3090 ± 0.4527, $p = 0.0001$) and day 4 (7.8917 ± 1.0080 vs 5.3419 ± 0.8607, $p < 0.0001$) (Fig. 10B). However, in $A\beta_{42\text{-}1}$ treated control group, rLV-miR-153 cells grew slower than rLV-miR cells and significantly slower on day 4 (8.9671 ± 0.7491 vs 13.7454 ± 0.4475, $p < 0.0001$) (Fig. 10B), compared with other days, which is consistent with the result of Fig. 10A. RLV-miR cells treated with $A\beta_{1\text{-}42}$ was more susceptible to Aβ toxicity than rLV-miR-153 cells, and miR-153 may decrease the susceptibility of cells to Aβ toxicity.

4. Discussion

MiRNAs can be envisioned as tools to modulate the differentiation and subspecification of neural stem cells and their progeny. Neurodegenerative diseases are often caused by impaired neurogenesis and synapse dysfunction [15]. Hence, understanding the mechanisms of miRNA-induced neuronal differentiation is necessary to improve neurogenesis and synaptic function in neurodegenerative diseases. Previous studies have shown that miRNAs function in the cytoplasm by targeting mRNA. Recent research confirmed that miRNA also works in the nucleus and cooperates with enhancer to activated gene expression [16,17]. We hope to provide an overview of the mRNA levels of miRNA-153 affecting neural differentiation of HT-22 cells. Our results suggested that miR-153 may promote neurogenesis by inducing neural cell adhesion/Ca^{2+} and the RTK(Ntrk2) signaling pathway, which may further affect the

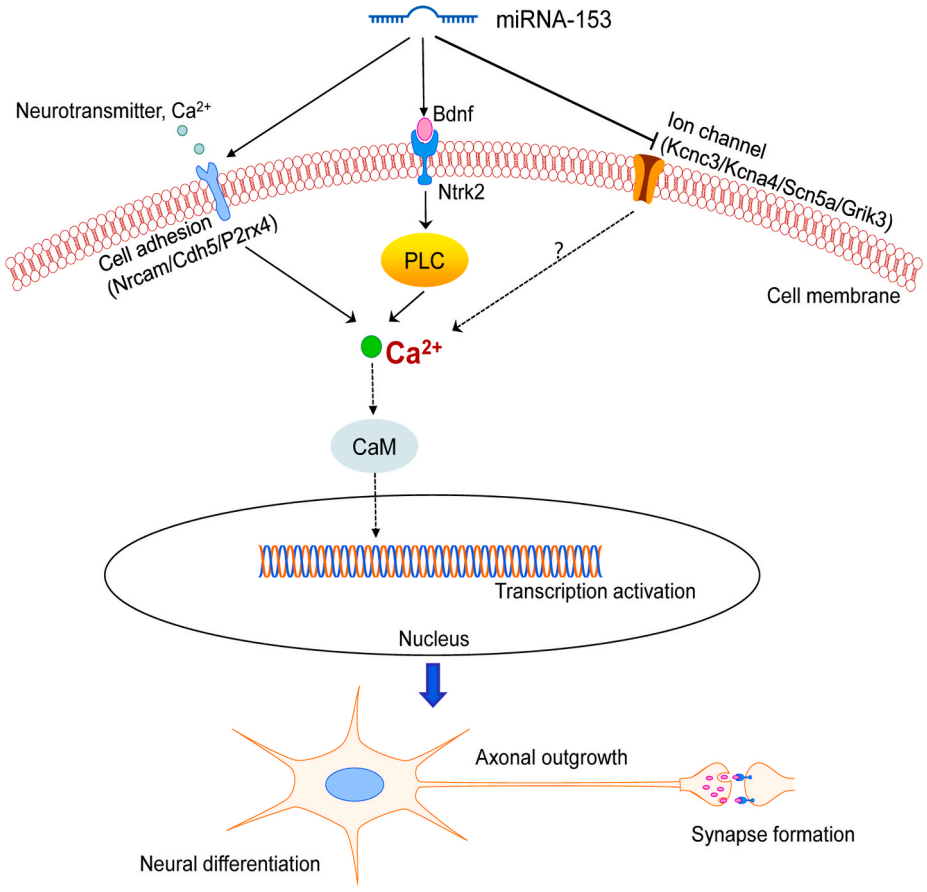

Fig. 11. Schematic diagram showing possible downstream signaling pathways of miR-153 overexpression.

synaptic function of damaged neurons and become a potential therapeutic target for neurodegenerative diseases. Fig. 11 illustrates the possible miRNA-153 downstream signaling pathways identified in this study.

CAMs play critical roles in many aspects of neurodevelopment, including axon growth and pathfinding, synapse formation, plasticity, learning and memory [18–20]. In this study, functional enrichment analysis indicated that the cell adhesion and calcium signaling pathways were significantly increased in rLV-miR-153 cells. Among the identified CAM-related hub genes, Cdh5 is a calcium dependent cadherins, and P2rx4 is a purinergic receptor and ion channel that is calcium-permeable and binds to cadherin, and Nrcam belongs to the immunoglobulin superfamily. In neural cells, the calcium signaling pathway can be activated when cadherins bind to Ca^{2+} and increase the intracellular Ca^{2+} concentration. Ca^{2+} can further transduce signals, including axonal outgrowth, guidance and synapse formation [21]. Cdh5 plays a role in endothelial adhere junction assembly and maintenance, and Fouda et al. [22] reported that Cdh5 showed strong expression in the hippocampus and cortical neurons of adult mice. HT-22 cells are a sub-line clone established from mouse hippocampus without forming synaptic connections [11]. Therefore, increased Cdh5 expression may affect the neural differentiation of rLV-miR-153 cells. P2rx4 contributes to synaptic strengthening during high-frequency stimulation [23] and facilitate Inhibitory GABAergic transmission [24]. Upregulation of P2rx4 in rLV-miR-153 cells may participate in synaptic functions. Nrcam is a member of the L1 family of neural cell adhesion molecules that are mainly distributed in growth cones and axons [25]. Cell adhesion of L1 subfamily members influences neurite outgrowth, axonal pathfinding, and neurite fasciculation during the development [26,27]. Ronn et al. [28] have reported that voltage-gated Ca^{2+}-channel blockers abolish NCAM-mediated neurite extension in hippocampal neurons. In addition, Nrcam forms a complex with membrane proteins, including voltage-gated sodium channels [29]. Notably, cluster 7 of BP (Fig. 4B) contained the hub genes of Scn1a, Nrcam and Scn1b. Both Scn1a and Scn1b are sodium channels that were significantly upregulated in rLV-miR-153 cells. This suggests that Nrcam upregualtion may mediate Ca^{2+} dependent signal transduction in rLV-miR-153 cells and may further affect the projection formation and increase branching, as observed in a previous study [10].

Transmembrane RTK signaling was another significantly upregulated pathway in rLV-miR-153 cells, as determined by enrichment analysis. Ntrk2 is a neurotrophic RTK and was among the identified upregulated hub genes of CC (cluster 12) (Fig. 5B) and MF (cluster 2) (Fig. 6B) in GO function analysis. Bdnf is a member of the neurotrophin family of secreted growth factors and binds with high affinity for Ntrk2. The interaction between Bdnf and Ntrk2 activates neurogenesis and dendritic growth [30–32]. qPCR analysis of Bdnf indicated a significant increase in Bdnf mRNA in rLV-miR-153 cells compared to that in control rLV-miR cells. Furthermore, phospholipase C (PLC) has been found to be activated through phosphorylation by Ntrk2 and further activates downstream Ca^{2+}-dependent calmodulin or enzymes and regulate neural development and function [33]. TrkB (Ntrk2)-mediated PLC signaling pathway is important for the initiation and maintenance of hippocampal long-term potentiation [34]. In this study, PLC activity was positively correlated in rLV-miR-153 cells using GSEA (Fig. 8C and. D). Wang et al. [35] reported that the activation of TrkB (Ntrk2) and its downstream signaling promoted neurite outgrowth and prevented Aβ-induced cell death in cultured neurons. Linking with the reduced susceptibility of rLV-miR-153 cells to Aβ peptide in our study, the upregulation of Ntrk2 may affect the response of rLV-miR-153 cells to Aβ treatment.

In addition to the upregulated genes, downregulated genes may also contribute to the overall effects of miR-153. Decreased DNA replication is a major function clustered in miR-153 cells. Neural differentiation couples the switch from expansion phase to neurogenic phase [36]. The attenuation of cell proliferation in miR-153 cells in this study may have been caused by decreased DNA replication and may have facilitated the conversion of cells from proliferation to neurogenesis. We further focused on the possible target genes of miR-153, and both GO function and GSEA analyses indicated the decreased ion channel activity in rLV-miR-153 cells. Kcnc3, Kcna4, Scn5a and Grik3 have been identified as ion channel-related genes. Ion channel expression substantially changes during differential neural differentiation [37]. Zhou et al. [38] found that knockdown of Kcna3 in NPCs also promoted neuronal differentiation. Ion channel expression is dynamic and contributes to the shifts in neural morphology and function during neurogenesis [39]. It is likely that the downregulation of ion channel activity in rLV-miR-153 cells regulates neurogenesis by balancing the dynamic membrane potential between channels.

The expression profiles of genes from the GDS3442 dataset were consistent with our results. Most NPCs are undifferentiated at E9.5, and start to differentiate into neurons at E11.5, and at E13.5 when neurogenesis peaks [40]. In the GDS3442 dataset, numerous gene expression changes occurred during mouse embryonic brain development, in which metabolism and cell cycle-related gene were downregulated when precursor cells switched from proliferation to neuronal differentiation (E9.5-E11.5), and neuron-specific gene products were up-regulated [14]. Especially, the expression change of the genes (Cdh5, Nrcam, P2rx4, Ntrk2, and Kcnc3), which we have identified in the study, displayed the consistent alteration from E9.5 to E13.5 in GDS3442. This suggests that miR-153 overexpression may reprogram gene expression and mimic neural differentiation.

Promoting neurogenesis and axonal remodeling is a useful therapeutic target for neurodegenerative diseases characterized by neuronal degeneration and loss. Here, we found the decreased susceptibility of rLV-miR-153 cells to $A\beta_{1\text{-}42}$ peptide in CCK8 assay, which indicated the likely protective role of miR-153 in treating AD. Qiao et al. [8] demonstrated that miR-153 overexpression promotes the neurogenesis of mouse neural stem cells, decreases miR-153 expression in aged mice and miR-153 overexpression can enhance the cognitive ability of aged mice. Taken together, for individuals who are already suffering from AD, miR-153 may mimic neural differentiation and activate neurogenic potentiality to halt neural death and repair synapses by increasing cell adhesion and the Bdnf/Ntrk2 signaling pathway. In addition, promoting neural cell adhesion and balancing ion channel activity with corresponding chemicals may be useful for treating neurodegenerative diseases.

Due to insufficient sample size, potential biases, and limited data, some issues regarding miR-153 neurogenesis control need to be further elucidated. First, gene expression induced by miR-153 must be confirmed in vivo, especially in an AD model. Secondly, the application of cell adhesion activators and ion channel inhibitors should be explored in vitro and in vivo in AD models. Third, the clinical applicability of miR-153 should be investigated, particularly in animal models of neurodegenerative diseases.

5. Conclusion

This study aimed to explore the possible molecular mechanism underlying miR-153 induced neural differentiation of HT-22 cells. It was observed that miR-153 induced the upregulation of neural cell adhesion-related molecules, the Bdnf/Ntrk pathway, and the downregulation of ion channel molecules, which is likely consistent with the change in expression during physiological neural development. This reveals that miR-153 may play an important role in neural differentiation and may provide a useful therapeutic direction for neurodegenerative diseases.

Funding

1. 2021 Scientific Research Project of Shanghai Municipal Commission of Health and Family Planning (NO.202140282)
2. Outstanding Leaders Training Program of Pudong Health Bureau of Shanghai (Grant No. PWR12020-03)

Data availability statement

All data generated or analyzed during this study are obtained from RNA sequencing which has been deposited in http://www.ncbi.nlm.nih with BioProject ID PRJNA793896. Gene expression profile is from GDS3442, in which Cdh5 (https://www.ncbi.nlm.nih.gov/geoprofiles/65839962), Nrcam (https://www.ncbi.nlm.nih.gov/geoprofiles/65836589), P2rx4 (https://www.ncbi.nlm.nih.gov/geoprofiles/65831531), Ntrk2 (https://www.ncbi.nlm.nih.gov/geoprofiles/65841311), Kcnc3 (https://www.ncbi.nlm.nih.gov/geoprofiles/65827987) and Clcn5 (https://www.ncbi.nlm.nih.gov/geoprofiles/65856782).

CRediT authorship contribution statement

Li Jiao: Writing – review & editing, Writing – original draft, Formal analysis, Conceptualization. **Zhang Junfang:** Methodology. **Li Yanna:** Methodology. **Jin Caixia:** Methodology. **Zhang Chen:** Conceptualization. **Jia Song:** Methodology. **Xu Jie:** Methodology. **Yan Xiaoli:** Methodology. **Gui Xin:** Methodology. **Xing Libo:** Methodology. **Wang Feng:** Conceptualization. **Lu lixia:** Conceptualization. **Xu Chunli:** Conceptualization. **Xu Lei:** Conceptualization.

Declaration of competing interest

The authors declare that they have no known competing financial interests or personal relationships that could have appeared to influence the work reported in this paper.

Appendix A. Supplementary data

Supplementary data to this article can be found online at https://doi.org/10.1016/j.heliyon.2024.e30204.

References

[1] K. Tsujimura, T. Shiohama, E. Takahashi, microRNA biology on brain development and neuroimaging approach, Brain Sci. 12 (10) (2022) 1366, https://doi.org/10.3390/brainsci12101366.
[2] V. Fernández, M.Á. Martínez-Martínez, A. Prieto-Colomina, A. Cárdenas, R. Soler, M. Dori, U. Tomasello, Y. Nomura, J.P. López-Atalaya, F. Calegari, V. Borrell, Repression of Irs2 by let-7 miRNAs is essential for homeostasis of the telencephalic neuroepithelium, EMBO J. 39 (21) (2020) e105479, https://doi.org/10.15252/embj.2020105479.
[3] N. Vo, M.E. Klein, O. Varlamova, D.M. Keller, T. Yamamoto, R.H. Goodman, S. Impey, A cAMP-response element binding protein-induced microRNA regulates neuronal morphogenesis, Proc Natl Acad Sci U S A 102 (45) (2005) 16426–16431, https://doi.org/10.1073/pnas.0508448102.
[4] S.T. Magill, X.A. Cambronne, B.W. Luikart, D.T. Lioy, B.H. Leighton, G.L. Westbrook, G. Mandel, R.H. Goodman, microRNA-132 regulates dendritic growth and arborization of newborn neurons in the adult hippocampus, Proc Natl Acad Sci U S A 107 (47) (2010) 20382–20387, https://doi.org/10.1073/pnas.1015691107.
[5] P.N. Nguyen, M. Kumar, E. Fedele, G. Bonanno, T. Bonifacino, MicroRNA alteration, application as biomarkers, and therapeutic approaches in neurodegenerative diseases, Int. J. Mol. Sci. 23 (9) (2022) 4718, https://doi.org/10.3390/ijms23094718.
[6] L.F. Sempere, S. Freemantle, I. Pitha-Rowe, E. Moss, E. Dmitrovsky, V. Ambros, Expression profiling of mammalian microRNAs uncovers a subset of brain-expressed microRNAs with possible roles in murine and human neuronal differentiation, Genome Biol. 5 (3) (2004) R13, https://doi.org/10.1186/gb-2004-5-3-r13.
[7] L. Stappert, L. Borghese, B. Roese-Koerner, S. Weinhold, P. Koch, S. Terstegge, M. Uhrberg, P. Wernet, O. Brüstle, MicroRNA-based promotion of human neuronal differentiation and subtype specification, PLoS One 8 (9) (2013), https://doi.org/10.1371/journal.pone.0059011, 10.1371.
[8] J. Qiao, J. Zhao, S. Chang, Q. Sun, N. Liu, J. Dong, Y. Chen, D. Yang, D. Ye, X. Liu, Y. Yu, W. Chen, S. Zhu, G. Wang, W. Jia, J. Xi, J. Kang, MicroRNA-153 improves the neurogenesis of neural stem cells and enhances the cognitive ability of aged mice through the notch signaling pathway, Cell Death Differ. 27 (2) (2020) 808–825, https://doi.org/10.1038/s41418-019-0388-4.
[9] J.M. Long, B. Ray, D.K. Lahiri, MicroRNA-153 physiologically inhibits expression of amyloid-β precursor protein in cultured human fetal brain cells and is dysregulated in a subset of Alzheimer disease patients, J. Biol. Chem. 287 (37) (2012) 31298–31310, https://doi.org/10.1074/jbc.M112.366336.
[10] C. Xu, C. Wang, Q. Meng, Y. Gu, Q. Wang, W. Xu, Y. Han, Y. Qin, J. Li, S. Jia, J. Xu, Y. Zhou, miR-153 promotes neural differentiation in the mouse hippocampal HT-22 cell line and increases the expression of neuron-specific enolase, Mol. Med. Rep. 20 (2) (2019) 1725–1735, https://doi.org/10.3892/mmr.2019.10421.

[11] J. Liu, L. Li, W.Z. Suo, HT22 hippocampal neuronal cell line possesses functional cholinergic properties, Life Sci. 84 (9–10) (2009) 267–271, https://doi.org/10.1016/j.lfs.2008.12.008.
[12] T. Hu, N. Chitnis, D. Monos, A. Dinh, Next-generation sequencing technologies: an overview, Hum. Immunol. 82 (11) (2021) 801–811, https://doi.org/10.1016/j.humimm.2021.02.012.
[13] S. Mirsadeghi, E. Shahbazi, K. Hemmesi, S. Nemati, H. Baharvand, J. Mirnajafi-Zadeh, S. Kiani, Development of membrane ion channels during neural differentiation from human embryonic stem cells, Biochem. Biophys. Res. Commun. 491 (1) (2017) 166–172, https://doi.org/10.1016/j.bbrc.2017.07.068.
[14] D. Hartl, M. Irmler, I. Römer, M.T. Mader, L. Mao, C. Zabel, M.H. de Angelis, J. Beckers, J. Klose, Transcriptome and proteome analysis of early embryonic mouse brain development, Proteomics 8 (6) (2008) 1257–1265, https://doi.org/10.1002/pmic.200700724.
[15] L. Culig, X. Chu, V.A. Bohr, Neurogenesis in aging and age-related neurodegenerative diseases, Ageing Res. Rev. 78 (2022) 101636, https://doi.org/10.1016/j.arr.2022.101636.
[16] M. Xiao, J. Li, W. Li, Y. Wang, F. Wu, Y. Xi, L. Zhang, C. Ding, H. Luo, Y. Li, L. Peng, L. Zhao, S. Peng, Y. Xiao, S. Dong, J. Cao, W. Yu, MicroRNAs activate gene transcription epigenetically as an enhancer trigger, RNA Biol. 14 (10) (2017) 1326–1334, https://doi.org/10.1080/15476286.2015.1112487.
[17] Y. Liang, Q. Zou, W. Yu, Steering against wind: a new network of NamiRNAs and enhancers, Dev. Reprod. Biol. 15 (5) (2017) 331–337, https://doi.org/10.1016/j.gpb.2017.05.001.
[18] T.C. Südhof, The cell biology of synapse formation, J. Cell Biol. 220 (7) (2021) e202103052, https://doi.org/10.1083/jcb.202103052.
[19] C.A. Short, E.A. Suarez-Zayas, T.M. Gomez, Cell adhesion and invasion mechanisms that guide developing axons, Curr. Opin. Neurobiol. 39 (2016) 77–85, https://doi.org/10.1016/j.conb.2016.04.012.
[20] W. Gulisano, A. Bizzoca, G. Gennarini, A. Palmeri, D. Puzzo, Role of the adhesion molecule F3/Contactin in synaptic plasticity and memory, Mol. Cell. Neurosci. 81 (2017) 64–71, https://doi.org/10.1016/j.mcn.2016.12.003.
[21] L. Sheng, I. Leshchyns'ka, V. Sytnyk, Cell adhesion and intracellular calcium signaling in neurons, Cell Commun. Signal. 11 (2013) 94, https://doi.org/10.1186/1478-811X-11-94.
[22] A.Y. Fouda, Z. Xu, S.P. Narayanan, R.W. Caldwell, R.B. Caldwell, Utility of LysM-cre and Cdh5-cre driver mice in retinal and brain research: an imaging study using tdTomato reporter mouse, Invest. Ophthalmol. Vis. Sci. 61 (3) (2020) 51, https://doi.org/10.1167/iovs.61.3.51.
[23] J.A. Sim, S. Chaumont, J. Jo, L. Ulmann, M.T. Young, K. Cho, G. Buell, R.A. North, F. Rassendren, Altered hippocampal synaptic potentiation in P2X4 knock-out mice, J. Neurosci. 26 (35) (2006) 9006–9009, https://doi.org/10.1523/JNEUROSCI.2370-06.2006.
[24] S. Hugel, R. Schlichter, Presynaptic P2X receptors facilitate inhibitory GABAergic transmission between cultured rat spinal cord dorsal horn neurons, J. Neurosci. 20 (6) (2000) 2121–2130, https://doi.org/10.1523/JNEUROSCI.20-06-02121.2000.
[25] F. Ango, G. di Cristo, H. Higashiyama, V. Bennett, P. Wu, Z.J. Huang, Ankyrin-based subcellular gradient of neurofascin, an immunoglobulin family protein, directs GABAergic innervation at purkinje axon initial segment, Cell 119 (2) (2004) 257–272, https://doi.org/10.1016/j.cell.2004.10.004.
[26] A. Usardi, K. Iyer, S.M. Sigoillot, A. Dusonchet, F. Selimi, The immunoglobulin-like superfamily member IGSF3 is a developmentally regulated protein that controls neuronal morphogenesis, Dev Neurobiol 77 (1) (2017) 75–92, https://doi.org/10.1002/dneu.22412.
[27] B.R. Shrestha, A. Burgos, W.B. Grueber, The immunoglobulin superfamily member basigin is required for complex dendrite formation in Drosophila, Front. Cell. Neurosci. 15 (2021) 739741, https://doi.org/10.3389/fncel.2021.739741.
[28] L.C. Rønn, S. Dissing, A. Holm, V. Berezin, E. Bock, Increased intracellular calcium is required for neurite outgrowth induced by a synthetic peptide ligand of NCAM, FEBS Lett. 518 (1–3) (2002) 60–66, https://doi.org/10.1016/S0014-5793(02)02644-3.
[29] S.M. Jenkins, V. Bennett, Ankyrin-G coordinates assembly of the spectrin-based membrane skeleton, voltage-gated sodium channels, and L1 CAMs at Purkinje neuron initial segments, J. Cell Biol. 155 (5) (2001) 739–746, https://doi.org/10.1083/jcb.200109026.
[30] S.H. Choi, E. Bylykbashi, Z.K. Chatila, S.W. Lee, B. Pulli, G.D. Clemenson, E. Kim, A. Rompala, M.K. Oram, C. Asselin, J. Aronson, C. Zhang, S.J. Miller, A. Lesinski, J.W. Chen, D.Y. Kim, H. van Praag, B.M. Spiegelman, F.H. Gage, R.E. Tanzi, Combined adult neurogenesis and BDNF mimic exercise effects on cognition in an Alzheimer's mouse model, Science 361 (6406) (2018) eaan8821, https://doi.org/10.1126/science.aan8821.
[31] Y. Li, B.W. Luikart, S. Birnbaum, J. Chen, C.H. Kwon, S.G. Kernie, R. Bassel-Duby, L.F. Parada, TrkB regulates hippocampal neurogenesis and governs sensitivity to antidepressive treatment, Neuron 59 (3) (2008) 399–412, https://doi.org/10.1016/j.neuron.2008.06.023.
[32] G.X. Ni, C. Liang, J. Wang, C.Q. Duan, P. Wang, Y.L. Wang, Astragaloside IV improves neurobehavior and promotes hippocampal neurogenesis in MCAO rats though BDNF-TrkB signaling pathway, Biomed. Pharmacother. 130 (2020) 110353, https://doi.org/10.1016/j.biopha.2020.110353.
[33] D.R. Kaplan, F.D. Miller, Neurotrophin signal transduction in the nervous system, Curr. Opin. Neurobiol. 10 (3) (2000) 381–391, https://doi.org/10.1016/S0959-4388(00)00092-1.
[34] L. Minichiello, A.M. Calella, D.L. Medina, T. Bonhoeffer, R. Klein, M. Korte, Mechanism of TrkB-mediated hippocampal long-term potentiation, Neuron 36 (1) (2002) 121–137, https://doi.org/10.1016/S0896-6273(02)00942-X.
[35] S. Wang, H. Yao, Y. Xu, R. Hao, W. Zhang, H. Liu, Y. Huang, W. Guo, B. Lu, Therapeutic potential of a TrkB agonistic antibody for Alzheimer's disease, Theranostics 10 (15) (2020) 6854–6874, https://doi.org/10.7150/thno.44165.
[36] M. Götz, W. Huttner, The cell biology of neurogenesis, Nat. Rev. Mol. Cell Biol. 6 (2005) 777–788, https://doi.org/10.1038/nrm1739.
[37] S. Mirsadeghi, E. Shahbazi, K. Hemmesi, S. Nemati, H. Baharvand, J. Mirnajafi-Zadeh, S. Kiani, Development of membrane ion channels during neural differentiation from human embryonic stem cells, Biochem. Biophys. Res. Commun. 491 (1) (2017) 166–172, https://doi.org/10.1016/j.bbrc.2017.07.068.
[38] Y.Y. Zhou, G.Q. Hou, S.W. He, Z. Xiao, H.J. Xu, Y.T. Qiu, S. Jiang, H. Zheng, Z.Y. Li, Psora-4, a Kv1.3 blocker, enhances differentiation and maturation in neural progenitor cells, CNS Neurosci. Ther. 21 (7) (2015) 558–567, https://doi.org/10.1111/cns.12402.
[39] S. Chi, Y. Cui, H. Wang, J. Jiang, T. Zhang, S. Sun, Z. Zhou, Y. Zhong, B. Xiao, Astrocytic Piezo1-mediated mechanotransduction determines adult neurogenesis and cognitive functions, Neuron 110 (18) (2022), https://doi.org/10.1016/j.neuron.2022.07.010, 2984-2999.e8.
[40] Y. Hirabayashi, Y. Gotoh, Stage-dependent fate determination of neural precursor cells in mouse forebrain, Neurosci. Res. 51 (4) (2005) 331–336, https://doi.org/10.1016/j.neures.2005.01.004.